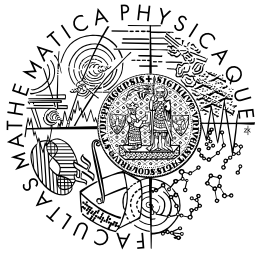

FACULTY
OF MATHEMATICS
AND PHYSICS
Charles University

BACHELOR THESIS

Róbert Králik

Neutrino physics at NOvA experiment

Institute of Particle and Nuclear Physics

Supervisor of the bachelor thesis:	RNDr. Karel Soustružník, Ph.D.
Study programme:	Physics
Study branch:	General Physics

Prague 2018

I declare that I carried out this bachelor thesis independently, and only with the cited sources, literature and other professional sources.

I understand that my work relates to the rights and obligations under the Act No. 121/2000 Sb., the Copyright Act, as amended, in particular the fact that the Charles University has the right to conclude a license agreement on the use of this work as a school work pursuant to Section 60 subsection 1 of the Copyright Act.

In ..... date ..... signature of the author

Title: Neutrino physics at NOvA experiment

Author: Róbert Králik

Institute: Institute of Particle and Nuclear Physics

Supervisor: RNDr. Karel Soustružník, Ph.D., Institute of Particle and Nuclear Physics

Abstract: This thesis describes neutrino phenomenology, with special aim at the phenomenon of sterile neutrinos and its experimental study, particularly in the NOvA experiment. Its aim is to clearly and comprehensibly introduce sterile neutrinos in context of historical and present measurements and discoveries. A brief summary of neutrino history is shown, as well as the theory of neutrino oscillations, including a description of matter effects and the effect of adding sterile neutrinos on the oscillation probabilities. NOvA experiment is presented, describing the neutrino source, the detectors and the used particle identification methods. Different experiments for the study of sterile neutrinos are listed and shortly described, with special concentration on the NOvA experiment and its measurement via the neutral-current channel. A detailed description of the first NOvA sterile neutrino result is provided, as well as the aspects of NOvA's current sterile neutrino analyses.

Keywords: neutrino, neutrino oscillations, sterile neutrinos, NOvA experiment

Název práce: Fyzika neutrin na experimentu NOvA

Autor: Róbert Králik

Ústav: Ústav částicové a jaderné fyziky

Vedoucí bakalářské práce: RNDr. Karel Soustružník, Ph.D., Ústav částicové a jaderné fyziky

Abstrakt: Táto práca popisuje fenomenológiu neutrín, so zameraním sa na sterilné neutrína a ich štúdiu na experimentoch, najmä na experimente NOvA. Cieľom je jasné a zrozumiteľné predstavenie sterilných neutrín v kontexte minulých a súčasných objavov a meraní. Je ukázané stručné zhrnutie histórie neutrín, rovnako ako popis teórie oscilácie neutrín, vrátane popisu vplyvu hmoty a vplyvu pridania sterilného neutrína na pravdepodobnosti oscilácií. Je predstavený experiment NOvA, kde sú popísané detektory, zdroj neutrín a metódy identifikácie častíc. V krátkosti sú predstavené rôzne experimenty študujúce sterilné neutrína, no hlavne meranie sterilných neutrín pomocou neutrálnych prúdov na experimente NOvA. Je ukázaný podrobný popis prvého výsledku štúdie sterilných neutrín na NOvA, ako aj aspekty súčasných analýz sterilných neutrín na NOvA.

Klíčová slova: neutríno, oscilácia neutrín, sterilné neutrína, NOvA experiment

I would like to thank my supervisor Karel Soustružník for introducing me to the beautiful world of neutrinos and for patience and understanding throughout this past semester.

I would also like to thank my dear friends and family, who have been a great support and help for me.

Contents

1. Introduction

When Wolfgang Pauli wrote to Geiger and Meitner during a meeting in Tübingen in December 1930, he "tried to connect a problem of the spin and statistics of the nucleus with the other of the continuous beta spectrum, without giving up the energy theorem, through the idea of a new neutral particle"(said Pauli in his 1957 lecture)[1]. In his letter he proposed a neutral particle with spin 1/2, obeying the exclusion principle, with mass of the same order of magnitude as the electron mass and, in any case, not larger than 0.01 proton mass. He named this particle neutron.[1]

This particle became well-known to physicists even before Pauli's first official publication of it, which happened at a conference held in 1933. Shortly after attending this conference, Enrico Fermi published his famous theory of beta decay, in which he already assumes the existence of the "neutrino". (He proposed this name for Pauli's "neutron" after Chadwick's discovery of neutron in 1932.)[1]

At the end of 1933 Francis Perrin concludes, that the mass of the neutrino should be zero and if it is so, than it does not exist in the nucleus but is created similarly to a photon. Enrico Fermi reached similar conclusion a year later.[2]

In 1937 Ettore Majorana proposed an idea, that neutrinos are particles which identify themselves with the corresponding antiparticle. Such neutrinos are now called Majorana's in contrast to Dirac's neutrinos.The problem with such particles is, that we cannot attribute a leptonic number to the Majorana neutrino as we do for Dirac's neutrino[2]. It was Giulio Racah who suggested testing this theory with neutrino-less double beta decay.[3]

Twenty years later in 1956, Cowan, Reines and co-workers experimentally proved the existence of the neutrino (actually of the electron neutrino ν_e) by measuring the cross section of the inverse beta decay using the anti-neutrino from a fission reactor at the Savannah River Plant (USA)[2]. The obtained energy averaged cross section was $\overline{\sigma} = (11 \pm 2.6) \times 10^{-44}\,\mathrm{cm}^2$[4], which agreed well with a cross section proposed by Bethe and Peierls as early as in 1934. In 1995 the Nobel Prize in physics was awarded jointly with one half to Frederick Reines for "the detection of the neutrino" (the other half was awarded to M. L. Perl "for the discovery of the tau lepton").[5]

By the 1960s there were accelerators making neutrinos, when Mel Schwartz designed the first neutrino beam, by having a proton beam strike a target and make pions, which would decay making neutrinos. A team led by Leon Lederman built a detector at Brookhaven designed to distinguish electrons and muons. Using an almost pure muon-neutrino ν_μ beam from an accelerator, they found 34 muons and only 8 electron showers[6], showing that what we now call the muon and electron neutrino are distinct particles. The experiment was repeated shortly afterwards at CERN with higher statistics and the result was confirmed[4]. Another Nobel Prize in physics for neutrino discoveries was awarded in 1988 jointly to Lederman, Schwartz and Steinberger for "the neutrino beam method and the demonstration of the doublet structure of the leptons through the discovery of the muon neutrino".[5]

Weak neutral currents, associated with the proposed existence of the Z-boson, were discovered in a bubble chamber experiment Gargamelle at CERN in 1973

and soon afterwards were these observations confirmed by several other experiments. The weak gauge bosons themselves, predicted by the Glashow-Weinberg-Salam model, were finally discovered at CERN in 1983[4]. In 1989 when the CERN LEP electron-positron collider was built with sufficient energy to study the Z boson, it was able to study the width of the Z. Since the Z mediates the weak interactions between all fermions, its width could be used to determine the number of light ($m_\nu < m_Z/2$) weakly interacting neutrinos and the number was found to be three.[1][6]

The third neutrino - the tau neutrino ν_τ was postulated to exist after the discovery of the τ lepton in 1975. The experimental evidence for it was published in 2000 as the DONUT experiment at Fermilab has found 4 ν_τ interactions, which is consistent with the Standard Model expectation.[8]

In 2002, the Nobel Prize in physics was divided and one half was awarded jointly to Davis and Koshiba for "pioneering contributions to astrophysics, in particular for the detection of cosmic neutrinos".[5]

1.1 Neutrino oscillations

The idea of neutrino oscillations was first proposed by Pontecorvo in 1957 for oscillations between neutrinos and anti-neutrinos, and later in 1962, after the discovery of muon neutrino, developed by Maki, Nakagawa and Sakata, for oscillations between neutrino flavors due to different neutrino flavor and mass eigenstates.[9]

In the 1960s John Bahcall and Ray Davis designed and constructed an experiment at the Homestake mine to measure neutrinos from the Sun. Bahcall predicted measurement of at least 6 SNU (Solar Neutrino Unit=10^{-36} captures per second per target atom) but measurements indicated less than 3 SNU[6]. This became the "*solar neutrino problem*". Other experiments joined in to study the solar neutrino flux. First was the Kamiokande experiment in Japan, originally built for nucleon decay. But both, Kamiokande and Davis experiments were only sensitive to the highest energy solar neutrinos. In order to measure the lower energy ones, two experiments using Gallium were mounted: Gallex in Italy and SAGE in the Soviet Union in the early 1990s. Those two experiments also measured fewer solar neutrinos than were expected, but the fraction they measured was larger than that of chlorine (Homestake) and water (Kamiokande) experiments. This was due to the MSW effect[6]. The MSW effect is describing oscillations in matter and was postulated in works by L. Wolfenstein in 1978 and by Mikheyev and Smirnov in 1986.[6] (More on the MSW effect in 2.3).

After establishing that neutral currents existed in addition to charged currents, neutrino scattering experiments focused on using energy and angular distribution of final state particles to study the structure of the target nucleons.[6]

In 1998 Super-Kamiokande, a water Cherenkov detector in Japan, provided compelling evidence for neutrino oscillations by measuring atmospheric neutrinos. First oscillation-studying accelerator-based experiments were K2K in Japan, MINOS in USA and CNGS in Europe. All these experiments confirmed the ex-

[1] Using standard model fits to LEP-SLC data, the number of neutrino types is determined to be $N = 2.984 \pm 0.008$.[7]

istence of neutrino oscillations as suggested by the atmospheric neutrino results. Reactor-based experiments, such as an experiment at the Chooz reactor in France and one at the Palo Verde reactor in Arizona did not see expected disappearance of $\nu_\mu \rightarrow \nu_e$, favouring the $\nu_\mu \rightarrow \nu_\tau$ explanation for the atmospheric neutrino anomaly.[6]

In 2015 the Nobel Prize in physics was awarded jointly to Takaaki Kajita and Arthur B. McDonald for "the discovery of neutrino oscillations, which shows that neutrinos have mass".[5]

Two experiments in underground mines in India and South Africa obtained first evidence for atmospheric neutrinos in 1965. Oscillation of these neutrinos was indicated when Cherenkov detectors IMB and Kamioka saw fewer ν_μ compared to ν_e than they expected. This was called the "too few nu mu" problem or "*atmospheric neutrino anomaly*".[6]

The LSND experiment took data from 1993 to 1998 and it has presented evidence for $\overline{\nu}_\mu \rightarrow \overline{\nu}_e$ oscillations at the $\Delta m^2 \sim 1\,\mathrm{eV}^2$ scale, while solar neutrino and reactor-antineutrino experiments have observed ν_e disappearance at $\Delta m^2 \sim 8 \times 10^{-5}\,\mathrm{eV}^2$ and atmospheric-neutrino and long-baseline accelerator-neutrino experiments, which have observed ν_μ disappearance at $\Delta m^2 \sim 3 \times 10^{-3}\,\mathrm{eV}^2$. Excess of events in the LSND has been named the "*LSND anomaly*".[10]

In the end of the century, there were three neutrino anomalies (atmospheric, solar and LSND), while there are only two independent squared neutrino mass differences in three neutrino oscillations model, which could explain only two of these anomalies[11]. Most global fits of neutrino data drop the LSND anomaly, because the other ones are considered as more solid. The LSND results require a much larger value of the mass splitting than the values in the three neutrino model. This might be due to mixing with a 4th neutrino, but such a neutrino would not couple to the Z boson as the other fermions do, and thus would be considered "*sterile*".[6]

2. Neutrino oscillations

The Standard Model neutrinos always interact in a definite flavor eigenstate, $|\nu_\alpha\rangle$, and propagate through space-time with an eigenstate of the free Hamiltonian, a definite mass state $|\nu_i\rangle$. These two states are not identical, which causes a phenomenon called neutrino oscillations, when a neutrino created in a specific flavor state might in-flight change into a different flavor state. This is an evidence, that neutrinos in fact do have non-zero masses.

If not stated otherwise, we will be using natural units, where $h/2\pi = c = 1$.

2.1 General formalism

The flavor states can be written as a superposition of the mass states via the unitary PMNS (Pontecorvo-Maki-Nakagawa-Sakata) matrix:

$$|\nu_\alpha\rangle = \sum_{i=1}^{n} U^*_{\alpha i} |\nu_i\rangle , \tag{2.1}$$

where n is the number of neutrinos. Same equation holds for anti-neutrinos, but with non-conjugated matrix.[1] [9]

The neutrinos are treated as plane waves, with the assumption that the neutrino is actually localized in space put in by hand. A careful, rigorous approach treating neutrinos as wave packets reproduces the same results.[9]

Neutrino in a state of flavor α is at time $t = 0$ in a superposition of mass eigenstates. Its time evolution is a time evolution of the individual mass states. In a vacuum this adds a phase factor to each mass state:

$$|\nu_\alpha(t)\rangle = \sum_i U^*_{\alpha i} e^{-i(E_i t - \boldsymbol{p_i}\cdot\boldsymbol{x})} |\nu_i\rangle . \tag{2.2}$$

We can make several assumptions according to the fact that neutrinos are ultra-relativistic. Replacing the time t by distance L, approximating energy of each eigenstate to be the same energy $E_i = E$ and expanding the momentum as $p_i = \sqrt{E^2 - m_i^2} \approx E - \frac{m_i^2}{2E}$. With these assumptions, equation for neutrino in position L simplifies as: [9]

$$|\nu_\alpha(L)\rangle = \sum_i U^*_{\alpha i} e^{-i m_i^2 L/2E} |\nu_i\rangle . \tag{2.3}$$

After expressing the mass eigenstate in terms of flavor eigenstates we get:

$$|\nu_\alpha(L)\rangle = \sum_{\alpha'} \sum_i U^*_{\alpha i} U_{\alpha' i} e^{-i m_i^2 L/2E} |\nu_{\alpha'}\rangle . \tag{2.4}$$

Probability amplitude that the original flavor state α has transitioned (or survived) as flavor state β is:

$$A_{\nu_\alpha \to \nu_\beta}(L) = \langle \nu_\beta | \nu_\alpha(L)\rangle = \sum_i U_{\beta i} U^*_{\alpha i} e^{-i m_i^2 L/2E}. \tag{2.5}$$

[1] Using a conjugated matrix is only a matter of convention, in some literatures it is possible to see the use of non-conjugated matrix for neutrinos and conjugated for anti-neutrinos.

Probability is then a square of this amplitude:

$$P_{\nu_\alpha \to \nu_\beta}(L) = |\langle \nu_\beta | \nu_\alpha(L) \rangle|^2 = \sum_{i,j} U_{\beta i} U^*_{\alpha i} U^*_{\beta j} U_{\alpha j} e^{-i\left(m_i^2 - m_j^2\right) L/2E}, \tag{2.6}$$

where the difference of the squared masses is usually denoted as $\Delta m^2_{ij} = m^2_i - m^2_j$. As can be seen, the observation of oscillations allows no absolute mass measurement, oscillations are only sensitive to Δm^2.

The complex exponential follows this identity:

$$e^{iA} = \cos A + i \sin A = 1 - 2\sin^2 \frac{A}{2} + i \sin A. \tag{2.7}$$

Rewriting the eq.2.6 as a sum of four sums using eq.2.7:

$$\begin{aligned} P_{\nu_\alpha \to \nu_\beta}(L) = &\sum_i U_{\beta i} U^*_{\alpha i} U^*_{\beta i} U_{\alpha i} + \sum_{i \neq j} U_{\beta i} U^*_{\alpha i} U^*_{\beta j} U_{\alpha j} \\ &- 2 \sum_{i \neq j} U_{\beta i} U^*_{\alpha i} U^*_{\beta j} U_{\alpha j} \sin^2\left(\Delta m^2_{ji} \frac{L}{4E}\right) \\ &+ i \sum_{i \neq j} U_{\beta i} U^*_{\alpha i} U^*_{\beta j} U_{\alpha j} \sin\left(\Delta m^2_{ji} \frac{L}{2E}\right). \end{aligned} \tag{2.8}$$

Applying the unitarity of mixing matrix U,

$$\sum_i U^*_{\alpha i} U_{\beta i} = \delta_{\alpha\beta}, \tag{2.9}$$

on the first two sums and further evaluating the other (for more in-detail computation see [12]), we can express the probability by:

$$\begin{aligned} P_{\nu_\alpha \to \nu_\beta}(L) = &\delta_{\alpha\beta} - 4 \sum_{i>j} \mathrm{Re}\left(U_{\beta i} U^*_{\alpha i} U^*_{\beta j} U_{\alpha j}\right) \sin^2\left(\frac{\Delta m^2_{ij} L}{4E}\right) \\ &+ 2 \sum_{i>j} \mathrm{Im}\left(U_{\beta i} U^*_{\alpha i} U^*_{\beta j} U_{\alpha j}\right) \sin\left(\frac{\Delta m^2_{ij} L}{2E}\right). \end{aligned} \tag{2.10}$$

In the further description we will use a common denotion:

$$\Delta m^2_{ij} \frac{L}{4E} \equiv \Delta_{ij}. \tag{2.11}$$

Eq. 2.10 simplifies more for the survival probability, when $\alpha = \beta$. Therefore:

$$U_{\beta i} U^*_{\alpha i} U^*_{\beta j} U_{\alpha j} = |U_{\alpha i}|^2 |U_{\alpha j}|^2, \tag{2.12}$$

what is a purely real term, so it's imaginary part vanishes and the probability simplifies to:

$$P_{\nu_\alpha \to \nu_\alpha}(L) = 1 - 4 \sum_{i>j} |U_{\alpha i}|^2 |U_{\alpha j}|^2 \sin^2 \Delta_{ij}. \tag{2.13}$$

In general the neutrino oscillation probability can violate CP or T symmetry, that is:[13]

$$P_{\nu_\alpha \to \nu_\beta} \neq P_{\overline{\nu}_\alpha \to \overline{\nu}_\beta}, \tag{2.14}$$

$$P_{\nu_\alpha \to \nu_\beta} \neq P_{\nu_\beta \to \nu_\alpha}. \tag{2.15}$$

On the other hand, the CPT theorem imposes and from eq.2.6 we can write:

$$P_{\nu_\alpha \to \nu_\beta} = P_{\overline{\nu}_\beta \to \overline{\nu}_\alpha}. \tag{2.16}$$

2.2 3 flavor model in a vacuum

Before taking into account sterile neutrinos, we shall discuss a case of Standard Model's 3 distinct neutrino flavors: electron ν_e, muon ν_μ and tau ν_τ. We will begin without considering effects of matter.

For the 3 flavors neutrino model, we have a 3×3 PMNS matrix, which can be parametrized as:[14]

$$U = \begin{pmatrix} U_{e1} & U_{e2} & U_{e3} \\ U_{\mu 1} & U_{\mu 2} & U_{\mu 3} \\ U_{\tau 1} & U_{\tau 2} & U_{\tau 3} \end{pmatrix} =$$

$$= \begin{pmatrix} 1 & 0 & 0 \\ 0 & c_{23} & s_{23} \\ 0 & -s_{23} & c_{23} \end{pmatrix} \begin{pmatrix} c_{13} & 0 & s_{13}e^{-i\delta} \\ 0 & 1 & 0 \\ -s_{13}e^{i\delta} & 0 & c_{13} \end{pmatrix} \begin{pmatrix} c_{12} & s_{12} & 0 \\ -s_{12} & c_{12} & 0 \\ 0 & 0 & 1 \end{pmatrix} \begin{pmatrix} 1 & 0 & 0 \\ 0 & e^{i\alpha} & 0 \\ 0 & 0 & e^{i\beta} \end{pmatrix}, \tag{2.17}$$

where $s_{ij} = sin\,(\theta_{ij})$ and $c_{ij} = cos\,(\theta_{ij})$. θ_{ij} are the mixing angles, δ is a Dirac phase and α and β are 2 Majorana phases (Majorana phases are non-zero only if neutrinos are Majorana particles). These phases cause CP violation and are of relevance in double β-decay.

Since one of the three mixing angles θ_{13} is found to be smaller than the others, the 3-flavor mixing case can be reduced to decoupled two neutrino flavor oscillation. In that case the transition probability for electron and muon neutrino is simplified:

$$P_{\nu_e \leftrightarrow \nu_\mu}\,(L/E) = sin^2\,(2\theta)\,sin^2\left(\frac{\Delta m^2 L}{2E}\right), \tag{2.18}$$

from which it is nicely shown that the amplitude of the oscillation probability depends on the corresponding mixing angle θ, while the frequency is affected by the mass splitting Δm^2, neutrino energy E and the distance the neutrino travels L.[15]

Solar neutrino experiments are most sensitive to the mixing angle θ_{12}, therefore it's called the solar mixing angle, whereas atmospheric experiments are most sensitive to the mixing angle θ_{23} - the atmospheric mixing angle.[15]

Also for historic reasons, Δm^2_{21} is known as the solar mass splitting and Δm^2_{32} as the atmospheric mass splitting. Since the sign of Δm^2_{32} is still unknown, a positive value of Δm^2_{32} is called the normal hierarchy and a negative is called the inverted hierarchy. This is schematically shown in fig.2.1[9]

2.3 Matter effects

The presence of matter can have a profound effects on the oscillation probabilities. That is due to the coherent effect of forward scattering from many particles in ordinary matter (namely protons, neutrons and electrons) on the propagation of a neutrino. This effect can be described as the presence of an effective potential [13]. The interactions can proceed with Z^0 boson exchange, that is via neutral current (NC), but this only provides an overall phase as all neutrino flavors participate in these interactions equally. However, the effective potential for ν_e is different,

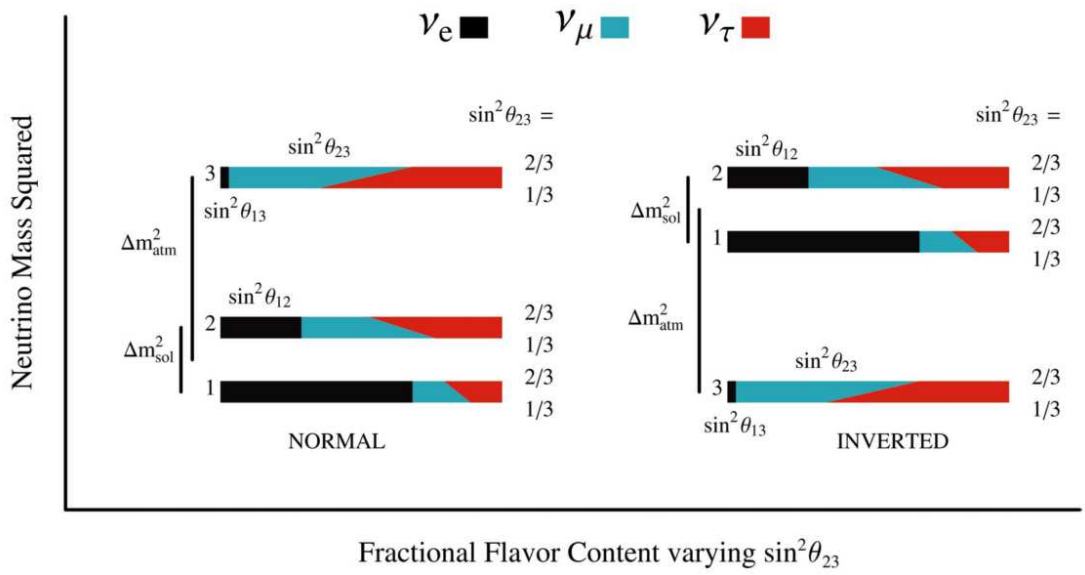

Figure 2.1: An illustration of different hierarchies of the mass splittings and a composition of flavor states in individual mass states corresponding to a 3 flavor model [16].

because the scattering can also proceed with W boson exchange, that is via charged current (CC) interactions with electrons (or positrons). The electrons contribute an additional potential term, $V_e = \pm\sqrt{2}G_F N_e$, where G_F is Fermi's constant, N_e is the electron density, the positive sign is for neutrinos and the negative for anti-neutrinos [9]. This effect is described by the Mikheyev-Smirnov-Wolfenstein effect, or the MSW effect. Neutrino interactions are visualized in fig.2.2.

The incoherent elastic and the quasi-elastic scattering, in which the states of the initial particles change in process are not of interest, since they have a negligible effect even in the center of the Sun, where the matter density is relatively high.[7]

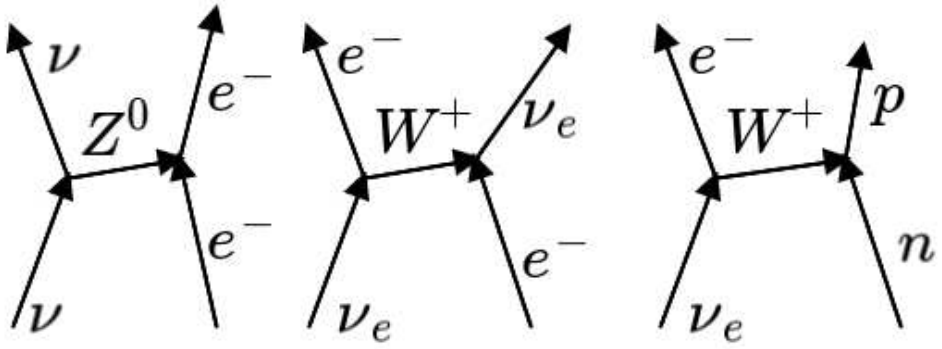

Figure 2.2: Feynman diagrams of different interactions of neutrino with matter particles - electron, proton or neutron.

In the presence of matter, the flavor evolution of neutrinos is described by an effective Hamiltonian, that is the sum of a free Hamiltonian and a matter induced term that includes the effective potential. The potential can be seen as having the effect of changing the mass of the neutrino. In fact we can write:[13]

$$E - V = \sqrt{p^2 + m^2} \cong + \frac{m^2}{2p} \tag{2.19}$$

and approximating $p \cong E$ one finds that the effect of the potential is equivalent to a shift in the squared mass:

$$m^2 \to m^2 + 2EV. \tag{2.20}$$

We will now consider only two flavor oscillation between ν_e and ν_x, where ν_x is a superposition of ν_μ and ν_τ. Adding the matter potential to the free Hamiltonian one obtains:[9] [13]

$$\mathcal{H} = U \begin{pmatrix} \frac{m_1^2}{2E} & 0 \\ 0 & \frac{m_2^2}{2E} \end{pmatrix} U^\dagger + \begin{pmatrix} \pm V_e & 0 \\ 0 & 0 \end{pmatrix}, \tag{2.21}$$

where a PMNS matrix for 2-flavor oscillations is:[9]

$$U = \begin{pmatrix} \cos\theta & \sin\theta \\ -\sin\theta & \cos\theta \end{pmatrix}. \tag{2.22}$$

Applying some trigonometric identities and dropping common diagonal terms, eq.2.21 simplifies to:[9]

$$\mathcal{H} = \frac{\Delta m^2}{4E} \begin{pmatrix} -\cos 2\theta \pm \frac{4E}{\Delta m^2} V_e & \sin 2\theta \\ \sin 2\theta & \cos 2\theta \end{pmatrix}. \tag{2.23}$$

This Hamiltonian can be re-diagonalized with another unitary transformation $\mathcal{H}_M = U_M^\dagger \mathcal{H} U_M$ with the following results:[9] [13]

$$\mathcal{H}_M = \frac{1}{2} \begin{pmatrix} -\frac{\Delta m_M^2}{2E} & 0 \\ 0 & \frac{\Delta m_M^2}{2E} \end{pmatrix}, \tag{2.24}$$

$$U_M = \begin{pmatrix} \cos\theta_M & \sin\theta_M \\ -\sin\theta_M & \cos\theta_M \end{pmatrix}, \tag{2.25}$$

where

$$\sin 2\theta_M = \frac{\sin 2\theta}{A_M}, \tag{2.26}$$

$$\Delta m_M^2 = \Delta m^2 A_M, \tag{2.27}$$

$$A_M = \sqrt{\left(\cos 2\theta \mp \frac{2EV_e}{\Delta m^2}\right)^2 + \sin^2 2\theta}. \tag{2.28}$$

where the negative sign in A_M is for neutrinos and the positive sign for anti-neutrinos.

The Hamiltonian takes the same form as a Hamiltonian in 2 flavor vacuum oscillations, but with modified effective masses. Likewise, U_M has the same form as the 2 neutrino PMNS matrix, so θ_M can be considered the effective mixing angle. As the effective potential goes to 0, the vacuum solution is recovered.[9]

In the case of 3 neutrinos, the same procedure is followed to diagonalize the Hamiltonian and obtain effective values for the various oscillation parameters.[9]

2.4 Current status

Many experiments studying neutrino oscillations provided enormous amount of data, which allows us to determine the oscillation parameters responsible for the solar ν_e oscillations (Δm^2_{21} and $\sin^2\theta_{12}$), for the dominant oscillations of the atmospheric ν_μ and $\overline{\nu}_\mu$ ($|\Delta m^2_{31}|$ and $\sin^2\theta_{23}$), and for the $\nu_\mu \to \nu_e$ and $\overline{\nu}_\mu \to \overline{\nu}_e$ oscillations (which is a case in the NOvA experiment) as well as the reactor $\overline{\nu}_e$ oscillations (θ_{13}). These parameters have been determined with an impressively high precision and the best fit values are shown in table 2.1. [7]

Parameter	best-fit	3σ	
Δm^2_{21}	$7.37 \times 10^{-5}\text{eV}^2$	$6.93 - 7.96$	
Δm^2_{31}	$2.56 \times 10^{-3}\text{eV}^2$	$2.45 - 2.69$	(normal mass hierarchy)
Δm^2_{32}	$2.54 \times 10^{-3}\text{eV}^2$	$2.42 - 2.66$	(inverted mass hierarchy)
$\sin^2\theta_{12}$	0.297	$0.250 - 0.354$	
$\sin^2\theta_{23}$	0.425	$0.371 - 0.615$	(normal mass hierarchy)
$\sin^2\theta_{23}$	0.589	$0.384 - 0.636$	(inverted mass hierarchy)
$\sin^2\theta_{13}$	0.0215	$0.0190 - 0.0240$	(normal mass hierarchy)
$\sin^2\theta_{13}$	0.0216	$0.0190 - 0.0242$	(inverted mass hierarchy)
δ/π	1.38	$2\sigma:\ 1.0 - 1.9$	(normal mass hierarchy)
δ/π	1.31	$2\sigma:\ 0.92 - 1.88$	(inverted mass hierarchy)

Table 2.1: Up-to-date best-fit values and 3σ allowed ranges of neutrino properties from 3-neutrino oscillation experiments. For the Dirac phase there is the best fit value and the 2σ allowed range. The paper was updated on June 5, 2018.[7]

It is also possible to set a cosmological bound on the sum of neutrino masses at 95% level of confidence (C.L.):[2][7]

$$\sum_j m_j < 0.170\,\text{eV}. \tag{2.29}$$

2.5 Sterile neutrinos

During the past quarter of a century, there have been several implications for the presence of one or more neutrinos at the eV scale in the mixing, additional to the already well established 3 light neutrinos[7]. Taking into account the number of

[2]This cosmological bound might not be valid if, e.g., the neutrino masses are generated dynamically at certain relatively late epoch in the evolution of the Universe.

light neutrinos coupled to the Z boson, these additional neutrinos must be sterile, i.e. not interact via the weak force.

Adding one sterile neutrino is often labelled as a 3+1 neutrino model and it is the simplest, most minimal extension to the Standard Model that explains the experimental data. There can be three different hierarchies, according to whether the additional mass splitting separates the solar and atmospheric mass splittings (the 2+2 hierarchy) or not (the 3+1 and 1+3 hierarchy). See fig.2.3 for visualisation. The former appears to be only marginally consistent with oscillation data, therefore it is not included in this study[17]. Also the 1+3 scheme with three massive neutrinos at the eV scale is strongly disfavoured by cosmological measurements and by the experimental bounds on neutrino-less double-β decay.[18]

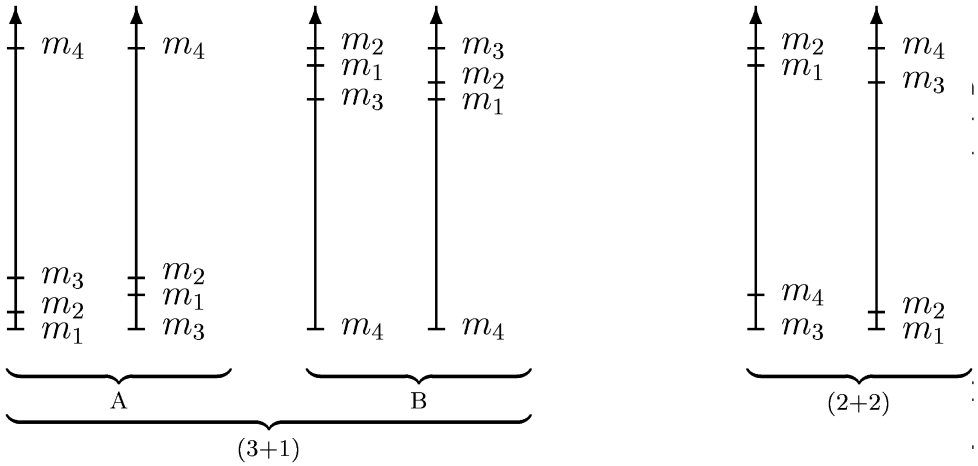

Figure 2.3: Depiction of possible hierarchies of neutrino masses in a three active plus one sterile neutrino model. Figure from [19].

However, theories presenting sterile neutrinos to explain the origin of neutrino masses do not require only one sterile neutrino. In fact, the tests show that the 3+2 neutrino model fits the short-baseline (SBL) data significantly better than the 3+1 model [17]. When moving from 1 to 2 sterile neutrinos the qualitative new feature is the possibility of CP violation already at short-baseline.[20]

For two sterile neutrinos, we would distinguish between a mass spectrum where Δm^2_{41} and Δm^2_{51} are both positive (3+2) and where one of them is negative (1+3+1). The phenomenology would be slightly different in the two cases.[20]

Adding more than two sterile neutrinos does not lead to any qualitatively new physical effects and the fit to the data does not improve significantly.[20]

In this thesis we shall concentrate on the 3+1 neutrino model, which introduces additional parameters compared to the 3 flavor model: θ_{14}, θ_{24} and θ_{34}, δ_{14} and δ_{24} and three mass splittings, with only one being independent (we will use Δm^2_{41}). We will label the neutrino mass eigenstates so that ν_1, ν_2, ν_3 are the ones that contribute mostly to the active flavor eigenstates and provide the mass squared difference required for "standard" three-flavor oscillations. The mass state ν_4 is mostly sterile and provides mass squared difference in the range $0.1\,\mathrm{eV}^2 < |\Delta m^2_{41}| < 10\,\mathrm{eV}^2$. We always assume $\Delta m^2_{41} > 0$, but the oscillation phenomenology for $\Delta m^2_{41} < 0$ would be the same.[20]

Since $|\Delta m^2_{41}| \gg |\Delta m^2_{32}| \gg |\Delta m^2_{21}|$, we can use following approximations:

$$\Delta m^2_{41} \sim \Delta m^2_{42} \sim \Delta m^2_{43}, \tag{2.30}$$

$$\Delta m^2_{31} = \Delta m^2_{32} + \Delta m^2_{21} \sim \Delta m^2_{32}. \tag{2.31}$$

The first approximation is sometimes referred to as the "quasi two neutrino approximation," or "one mass scale dominance"[17]. Applying these to general probability equations (2.10 and 2.13) and neglecting Δm^2_{21} for its relative small effects, we can denote probabilities useful in the sterile neutrino studies at NOvA experiment, which uses beam of ν_μ and/or $\overline{\nu}_\mu$. We also use unitarity of U (eq. 2.9) and the denotion from 2.11. We have used the same notation as in [9].

The survival probability of ν_μ is:

$$\begin{aligned} P_{\nu_\mu \to \nu_\mu}(L) &\approx 1 - 4|U_{\mu 4}|^2 \left(|U_{\mu 1}|^2 + |U_{\mu 2}|^2 + |U_{\mu 3}|^2\right) \sin^2 \Delta_{41} \\ &\quad - 4|U_{\mu 3}|^2 \left(|U_{\mu 1}|^2 + |U_{\mu 2}|^2\right) sin^2 \Delta_{31} \\ &\approx 1 - 4|U_{\mu 4}|^2 \left(1 - |U_{\mu 4}|^2\right) \sin^2 \Delta_{41} \\ &\quad - 4|U_{\mu 3}|^2 \left(1 - |U_{\mu 4}|^2 - |U_{\mu 3}|^2\right) \sin^2 \Delta_{31}. \end{aligned} \tag{2.32}$$

And the probability that the ν_μ does not oscillate into sterile neutrino (or that it survives as one of the active neutrino flavors) is:

$$\begin{aligned} 1 - P_{\nu_\mu \to \nu_s}(L) &\approx 1 + 4\mathrm{Re}\left(C_{41,42,43}\right) \sin^2 \Delta_{41} + 4\mathrm{Re}\left(C_{31,32}\right) \sin^2 \Delta_{31} \\ &\quad - 2\mathrm{Im}\left(C_{41,42,43}\right) \sin 2\Delta_{41} - 2\mathrm{Im}\left(C_{31,32}\right) \sin 2\Delta_{31}, \end{aligned} \tag{2.33}$$

where

$$\begin{aligned} C_{41,42,43} &= U_{s4} U^*_{\mu 4} \left(U^*_{s1} U_{\mu 1} + U^*_{s2} U_{\mu 2} + U^*_{s3} U_{\mu 3}\right) \\ &= U_{s4} U^*_{\mu 4} \left(-U^*_{s4} U_{\mu 4}\right) = -|U_{s4}|^2 |U_{\mu 4}|^2, \end{aligned} \tag{2.34}$$

what is a purely real term, therefore it's imaginary part is equal zero.

Also

$$\begin{aligned} C_{31,32} &= U_{s3} U^*_{\mu 3} \left(U^*_{s1} U_{\mu 1} + U^*_{s2} U_{\mu 2}\right) \\ &= -U_{s3} U^*_{\mu 3} \left(U^*_{s3} U_{\mu 3} + U^*_{s4} U_{\mu 4}\right) \\ &= -|U_{s3}|^2 |U_{\mu 3}|^2 - U_{s3} U^*_{s4} U^*_{\mu 3} U_{\mu 4}. \end{aligned} \tag{2.35}$$

Getting:

$$\begin{aligned} 1 - P_{\nu_\mu \to \nu_s}(L) &\approx 1 - 4|U_{s4}|^2 |U_{\mu 4}|^2 \sin^2 \Delta_{41} - 4|U_{s3}|^2 |U_{\mu 3}|^2 \sin^2 \Delta_{31} \\ &\quad - 4\mathrm{Re}\left(U_{s3} U^*_{s4} U^*_{\mu 3} U_{\mu 4}\right) \sin^2 \Delta_{31} \\ &\quad + 2\mathrm{Im}\left(U_{s3} U^*_{s4} U^*_{\mu 3} U_{\mu 4}\right) \sin 2\Delta_{31}. \end{aligned} \tag{2.36}$$

This probability is depicted in fig.2.4.

Oscillation physics including sterile neutrinos can be described by a rectangular mixing matrix $U_{\alpha i}$, where $\alpha = e, \mu, \tau$ and $i = 1, ..., 3 + s$ (s is the number of added sterile neutrinos) and

$$\sum_i U^*_{\alpha i} U_{\beta i} = \delta_{\alpha \beta}. \tag{2.37}$$

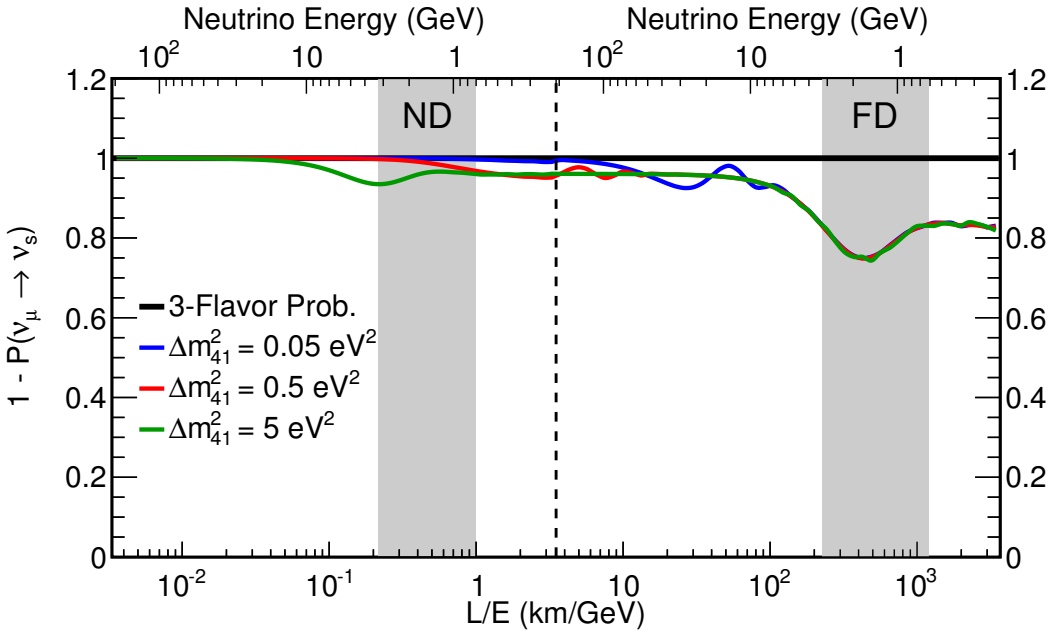

Figure 2.4: The probability that ν_μ does not oscillate into sterile neutrino as a function of L/E (distance/energy) for three different Δm^2_{41} compared to a 3-flavor case. Regions corresponding to NOvA's near detector (ND) and far detector (FD) are highlighted. Figure is from NOvA's internal database.

It can be convenient to complete the $3 \times (3+s)$ rectangular matrix by s rows to an $n \times n$ unitary matrix with $n = 3+s$ and with the following parametrization from [21]

$$U = O_{34} V_{24} V_{14} O_{23} V_{13} O_{12}, \tag{2.38}$$

where O_{ij} represents a real rotation matrix by an angle θ_{ij} in the ij plane and V_{ij} represents a complex rotation by an angle θ_{ij} and a phase φ_{ij} (analogically to 3 flavor model parametrization $U = O_{23} V_{13} O_{12}$, see eq.2.17). This particular ordering is a an arbitrary convention.

Note that we have expressed needed probabilities using only four elements of the mixing matrix: U_{s3}, U_{s4}, $U_{\mu 3}$ and $U_{\mu 4}$. These and other useful matrix elements can be expressed in oscillation parameters as:

$$\begin{aligned}
U_{\mu 3} &= -s_{14} s_{24} s_{13} e^{-i\delta_{13}} e^{-i\delta_{24}} e^{i\delta_{14}} + c_{24} s_{23} c_{13}, \\
U_{\mu 4} &= c_{14} s_{24} e^{-i\delta_{24}}, \\
U_{s3} &= -c_{34} c_{24} s_{14} s_{13} e^{-i\delta_{13}} e^{i\delta_{14}} - c_{13} c_{34} s_{24} s_{23} e^{i\delta_{24}} - c_{13} c_{23} s_{34}, \\
U_{s4} &= c_{14} c_{24} c_{34}, \\
U_{\tau 4} &= c_{14} c_{24} s_{34}.
\end{aligned}$$

2.6 Matter effect for sterile neutrinos

As was stated in chapter 2.3, without presence of sterile neutrino, the NC interaction in matter provides only an overall phase to the neutrino propagation, since all active neutrinos participate in this kind of interaction. That is however not true for sterile neutrinos, which do not interact via weak (or any Standard Model)

force. We must therefore add another term to the effective potential from 2.3, expressing the effect of NC forward scattering of active (non-sterile) neutrinos from matter (mostly electrons, protons and neutrons). The contribution from electrons and protons cancels each other out due to equal densities, but the effect of the neutrons remain.[9]

The expressed full effective potential in matrix notation:[9]

$$V = V_{CC} + V_{NC} = \sqrt{2}G_F \left[\pm N_e \text{diag}\left(1,0,0,0,...\right) \mp \frac{1}{2} N_n \text{diag}\left(1,1,1,0,...\right) \right]. \tag{2.39}$$

3. NOvA experiment

NOvA experiment stands for NuMI Off-axis ν_e Appearance experiment. As its name suggests, it is designed to search for muon to electron neutrino oscillations by comparing electron neutrino rates at Near Detector (ND) with those observed at Far Detector (FD), while both detectors are positioned off the main axis of the NuMI neutrino beam[22]. Its primary aims are to measure θ_{13}, to determine whether CP is violated in the lepton sector, and to resolve the neutrino mass hierarchy (i.e. to measure the sign of Δm^2_{32}), that can only be determined through the measurement of matter effects, for which NOvA has been optimized with its exceptionally long baseline (longest baseline in operation).[14]

NOvA is an experiment under Fermi National Accelerator Laboratory (Fermilab), the second generation experiment on NuMI beam line (after the MINOS experiment), positioned directly at Fermilab site in Batavia, Illinois (the accelerator and the near detector, which are approximately 1 km apart) and also 810 km from Fermilab, near Ash River, Minnesota (the far detector)[14]. In the beginning it was scheduled to run for 6 years, equally split between neutrino and antineutrino flux, with a total of 36×10^{20} protons delivered by NuMI[22]. Physics run started in February, 2014, and first result of ν_e appearance measurement were reported in 2016[7]. It will most probably continue on until the launch of the DUNE experiment.

NOvA experiment currently has 242 scientists and engineers from 48 universities and laboratories. Charles University joined in in 2011 and our group consists of 5 people including me.[23]

3.1 The NuMI beam

First build for MINOS and COSMOS experiments (latter was later withdrawn), the NuMI, or the Neutrino at the Main Injector neutrino beam facility has presently the world's most powerful neutrino beam[24]. It produces neutrinos by steering a 120 GeV proton beam with intensities of 700 kW, on a 1.2 meter-long graphite target through a collimating baffle[21]. The hadrons produced are focused in the desired direction and selected based on the sign of their charge by two magnetic horns (coaxial toroidal magnets) and then enter a 675 m long decay volume. Pions and kaons constitute a major portion of the hadrons and predominantly decay via the modes $\pi^+ \to \mu^+ + \nu_\mu$ and $K^+ \to \mu^+ + \nu_\mu$ yielding a ν_μ beam.[24]

The horn appears to the incoming positive hadrons as a focusing lens with a focal length proportional to their momentum therefore it provides flexibility in choosing energy at which secondary particles are best focused by adjusting the target to horn distance and also the separation between the two horns. The design accommodates three Horn 2 positions corresponding to low, medium and high energy. NOvA experiment makes use of the medium energy positioning, while MINOS experiment used the low energy positioning. The horn current can be reversed allowing sign selection of the hadrons focused to produce an antineutrino-enhanced beam (RHC=Reversed Horn Current), instead of predominantly neutrino beam (FHC=Forward Horn Current)[24]. NOvA alternates between FHC

and RHC mode, which can be seen on fig.3.1.

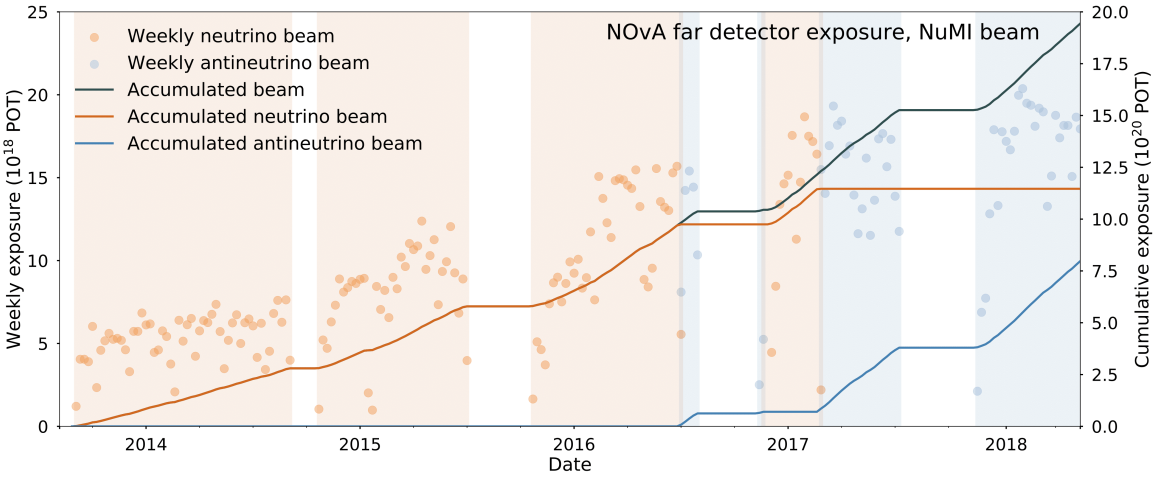

Figure 3.1: Weakly NOvA FD exposure shown as dots as well as cumulative NOvA FD exposure shown as lines in POT (Protons On Target) units from the beginning of NOvA physics run to early 2018. The graph shows exposures for both neutrinos and antineutrinos corresponding to FHC mode or RHC mode respectively, as well as the total cumulative exposure. Figure is from NOvA's internal database.

The off-axis location means that both NOvA detectors are sited 14.6 mrad off the NuMI beam axis, in contrast to the MINOS Far Detector. This is because at around 14 mrad, the energy of the neutrino does not have a strong dependence on the energy of the parent pion (fig. 3.2), and also at this angle, the medium energy beam produces a narrow energy beam with approximately five times more neutrinos at 2 GeV (fig. 3.3), which is well-matched to the oscillation maximum expected to be at 1.6 GeV, thus maximizing the experiment's neutrino oscillation sensitivity. In addition to the increased flux, the narrowness of the off-axis spectra enhances background rejection.[22]

The beam is extracted for 10 μs every 1.33 s and is composed primarily of ν_μ (in FHC mode). Simulation predicts small contaminations of 1.8% $\overline{\nu}_\mu$ and 0.7% $\nu_e + \overline{\nu}_e$ in the $1 - 3$ GeV energy range[21]. Contamination of $\overline{\nu}_\mu$ by ν_μ in RHC mode is considerably higher and can vary from 2% to 20% in said energy range.[25]

The experimental composition of the NuMI beam facility is illustrated in fig.3.4.

3.2 The detectors

NOvA has two detectors, functionally-identical tracking calorimeters, composed of cells filled with a mineral oil-based liquid scintillator doped with 5% pseudocumene [21]. The liquid scintillator comprises 62% of the total detector mass[22]. The cells are 3.56 cm by 5.59 cm constructed from PVC and loaded with titanium dioxide to enhance reflectivity[23]. The FD (ND) cells are 15.3 (3.8) m long and

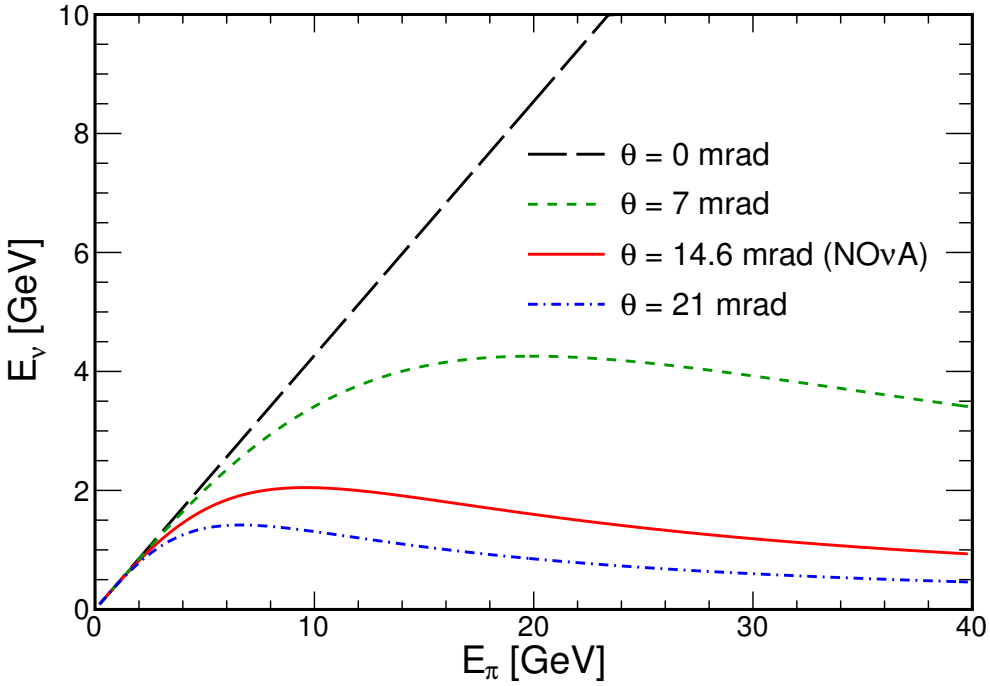

Figure 3.2: Energy dependencies of the neutrino on the parent pion for 4 different angles from the main axis. The angle coloured red is the one used in the NOvA experiment, where both ND and FD are positioned 14.6 mrad off-axis of the neutrino beam. Figure is from NOvA's internal database.

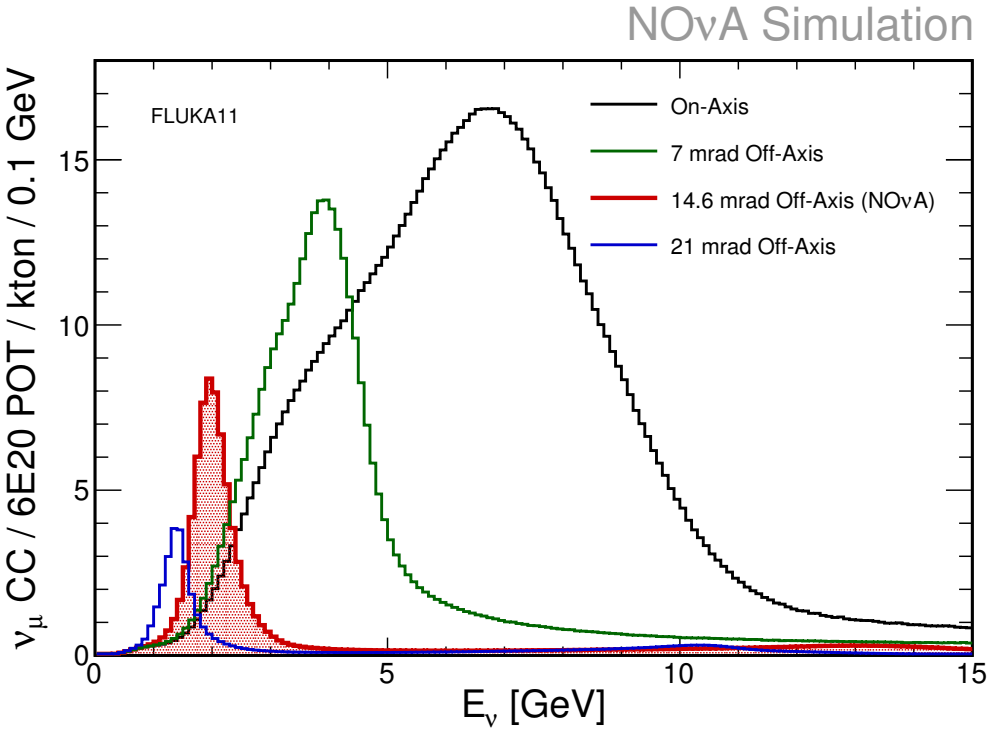

Figure 3.3: Dependence of the neutrino intensity on its energy for four different angles off the main axis. The peak coloured red is the one used in the NOvA experiment. Figure is from NOvA's internal database.

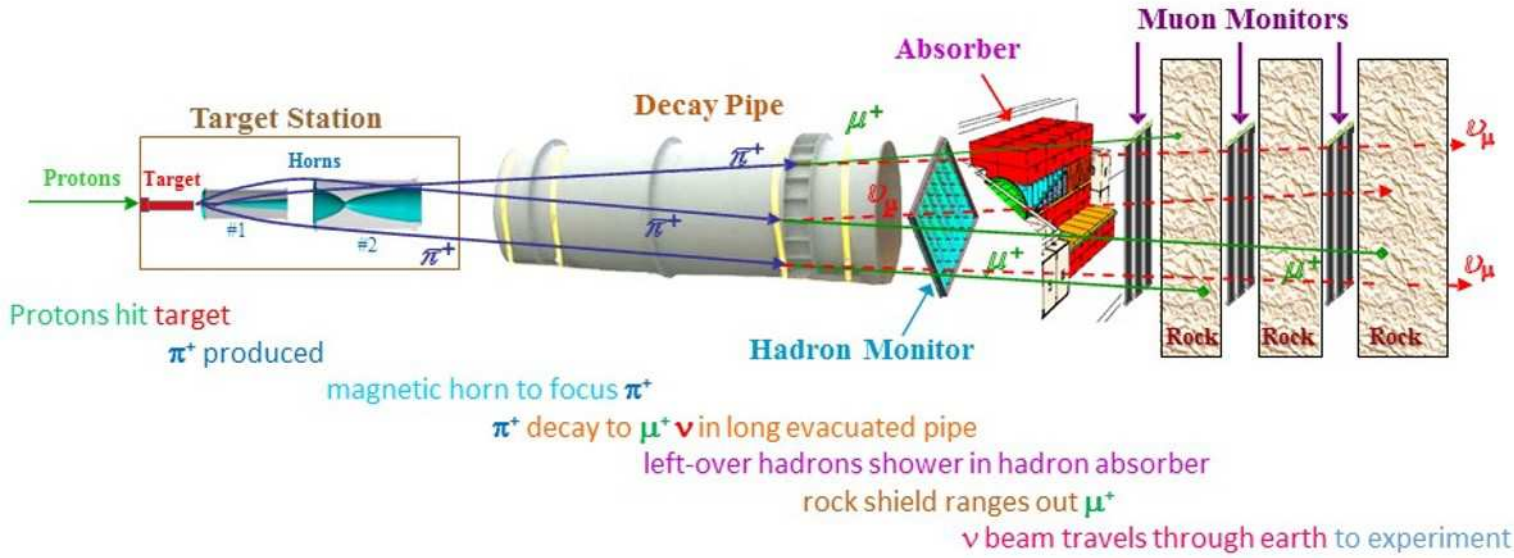

Figure 3.4: The schematic of the NuMI beam facility. The beam travels from left to right. The individual components shown are not to scale. Protons originate as H^- ions, which are converted into protons in the Booster, sent to the main injector, where they are finally accelerated to 120 GeV, bent downward by 58 mrad and transported 350 m to the 1.2 m long NuMI target. The protons are incident on the graphite target and the produced hadrons are focused by two magnetic horns, located in about 40 m long target hall, with about 19 m separation between the two horns. Hadrons then enter a 675 m long decay pipe made of steel, with 2 m diameter, which serves as vacuum or low density environment for the mesons to propagate and decay into tertiary mesons, charged leptons and neutrinos. A hadron monitor is located at the end of the decay volume just in front of the 5 m thick aluminium, steel and concrete absorber to record the profile of the residual hadrons. Of the particles interacting in the absorber, the principal component (approximately 80%) is the proton beam that has not interacted. The remainder are mainly mesons which have not decayed in the pipe or secondary protons. The absorber not only stops most of the particles still remaining in the beam but also acts as a shield against radiation. Muons and neutrinos deposit little or no energy in the absorber and continue into unexcavated rock with three muon monitors allowing measurement of the residual muon flux. The 240 m of rock following the absorber stops the muons remaining in the beam but allows the neutrinos to pass [24]. Figure is from NOvA's internal database.

a total of 344,064 (20,192) cells are organized into 896 (214) planes, arranged so that the cells alternate between horizontal and vertical orientations, relative to the beam axis, to enable 3-dimensional reconstruction.[21] [23]

The longitudinal segmentation (one cell) corresponds to 0.15 X_0 (radiation length) and the Moliere radius is 10 cm, ideal for the identification of electron-type neutrino events[26]. Charged particles from neutrino interactions or cosmic ray muons will emit scintillation light in the scintillator. The scintillation light is collected by a loop of 0.7 mm diameter wavelength shifting fibres (WLS) and a 32-pixel Avalanche Photodiode (APD) attached to the fibres converts the light pulse into electrical signals[26]. Using photo-detectors, we can determine a flavor and energy of the neutrino, which interacted with detector atom.

The data from APDs are concentrated by the Data Acquisition (DAQ) system which records them for further processing. The data flows through the front end boards, where it is continuously digitized, into the data concentrator modules, which consolidate it into 5 µs time slices, into the buffer nodes. There the data is buffered for a minimum of 20 s, waiting for the spill trigger, which is required to arrive within the buffering time to determine if the hits occurred in or out spill. The data from buffer nodes continues to the datalogger, where it is merged to form an event and than archived on disk or tape.[26]

The 14 metric-kiloton FD is sank 16 m into earth in granite rock. The excavated rock is used as a cosmic ray shield on the above surface sides of the building. The roof of the building over the detector is a 3 m overburden of concrete and barite (barium sulfate) which blocks most of the electromagnetic and hadronic components of cosmic ray secondaries[21] [22]. The 330 metric-ton ND is placed in an underground cavern adjacent to the NuMI experiment tunnel on the Fermilab site[22]. Both near and far detectors are placed at the same off-axis angle. Their scale and composition is depicted in fig.3.5.

Particle identification

Particle identification (PID) starts with the clustering of energy deposits that are close in space and time to form the event. Applying a Hugh transform to the cluster and determining three-dimensional vertex from a fit to the resulting lines' most likely common origin leads to reconstruction of individual particles within the event. The spatial locations of energy deposits are clustered around the vertex into prongs (clusters with defined starting point and direction), each containing deposits attributed to a final-state particle.[21]

To identify different neutrino interactions, NOvA uses a machine learning algorithm known as a convolutional neural network named Convolutional Visual Network (CVN). This algorithm identifies neutrino interactions based on their topology, without the need for detailed reconstruction. It extracts classification features using a series of transformations to the pattern of energy deposits within the detector, and then uses these features to determine the likelihood that a particle interaction is of a particular type. The CVN simultaneously provides classifiers for multiple interaction types (namely ν_e CC, ν_μ CC, ν_τ CC and ν NC) and since it views the entire topology, it can minimize misidentification between them.[28]

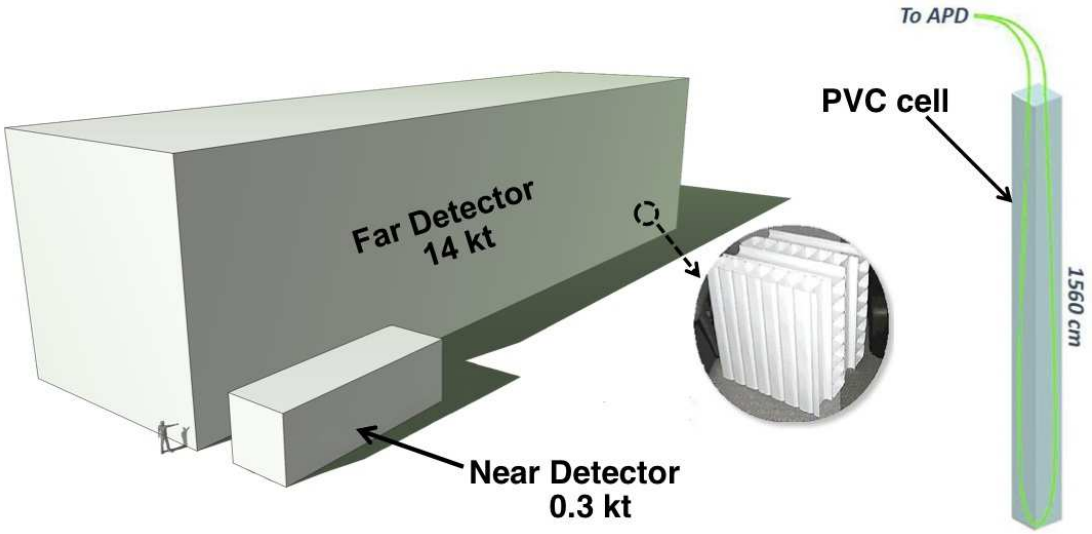

Figure 3.5: Scale and composition of the NOvA detectors. Their dimensions are: Far detector $15.23\,\mathrm{m} \times 15.14\,\mathrm{m} \times 59.62\,\mathrm{m}$; Near detector $3.83\,\mathrm{m} \times 3.81\,\mathrm{m} \times 15.87\,\mathrm{m}$. The detectors are composed of planes made of PVC cells, which alternate between horizontal and vertical orientations, relative to the beam axis. Each cell is filled with liquid scintillator and contains a loop of wavelength shifting fibre attached to an avalanche photodiode [23]. Figure is from [27].

4. Search for sterile neutrinos

4.1 Experimental indications

Hints for the existence of sterile neutrinos have been obtained in short-baseline $\nu_e/\overline{\nu}_e$ appearance experiments (LSND, MiniBooNE), from reactor neutrino experiments and from solar neutrino experiments.[7]

On the other hand, several other short and long baseline searches have found no evidence for light ν_s states and place strong constraints on their existence[21]. This creates a strong tension mainly between $\nu_\mu \to \nu_e$ and $\nu_\mu \to \nu_\mu$ channels (as well as the corresponding anti-neutrino channels).[29]

Although we only consider 3+1 scenario (adding just one sterile neutrino at the eV scale), it had been shown that adding more neutrinos does not relax the tension[29]. Other explanations include 3+N neutrino oscillation models involving three active neutrinos and N additional sterile neutrinos, resonant neutrino oscillations, Lorentz violation, sterile neutrino decay, sterile neutrino non-standard interactions, and sterile neutrino extra dimensions.[30]

4.1.1 Electron (anti)neutrino disappearance experiments

In the $\nu_e/\overline{\nu}_e$ disappearance channel, the most important constraints on sterile neutrinos come from short baseline ($L \leq 1\,\mathrm{km}$) reactor experiments, but also from solar and radioactive source experiments.[29]

Reactor experiments

After the re-evaluation of the reactor antineutrino spectra in 2011, the study of light sterile neutrinos got a new momentum. These new calculation indicate flux about 3.5% higher than previous estimates [31] and after re-analysing of 19 reactor experiments with baselines of 100 metres and less, a deficit in the measured neutrino flux was revealed, thus creating the so-called reactor antineutrino anomaly.[32]

Latest results of the combined analysis of experiments DANSS and NEOS disfavour the no-oscillation hypothesis with respect to sterile neutrino oscillations at a significance of 3.3σ. These results are completely independent of reactor neutrino flux predictions and are only based on bin-by-bin spectral comparison between two detector locations in DANSS, and between the spectra observed in NEOS and Daya Bay.[29]

The deviation of the energy spectra from the predictions appears to be similar at the near and far detectors and to be positively correlated with the reactor power. This strongly disfavours a possible explanation in terms of new physics (i.e. super-light sterile neutrinos).[31]

It has also been pointed out, that said anomaly could be explained by a miscalculation of the ^{235}U reactor antineutrino flux.[31]

Solar neutrino experiments

Another anomaly, titled "gallium anomaly", was found in the 1990s in the solar neutrino experiments GALLEX and SAGE using high intensity radioactive sources. The measured deficit has statistical significance about 3σ [32]. However, a systematic error in the Ga extraction efficiency or in the theoretical estimate of the cross-section also remain possible explanations.[31]

Global fit

Combining all the data on $\nu_e/\overline{\nu}_e$ disappearance yields a best fit $\Delta m^2_{41} \approx 1.3\,\mathrm{eV}^2$, in agreement with the reactor-only analyses and we can conclude, that global $\nu_e/\overline{\nu}_e$ disappearance data show a robust hint in favour of sterile neutrinos at the 3σ level.[29]

4.1.2 Electron (anti)neutrino appearance experiments

Accelerator experiments with baseline to neutrino energy ratio $L/E_\nu \sim 1\,\mathrm{m/MeV}$ can effectively probe neutrino oscillations occurring at $\Delta m^2 \sim 1\,\mathrm{eV}^2$ [31]. This channel was also the first to hint towards light sterile neutrinos, namely in the LSND experiment. This hint was later reinforced with MiniBooNE experiment, but experiments such as KARMEN, NOMAD, E776, ICARUS and OPERA have not been able to confirm those findings, albeit not ruling them out either.[29]

LSND and KARMEN

The Liquid Scintillation Neutrino Detector (LSND) searched for neutrino oscillations in the $\overline{\nu}_\mu \to \overline{\nu}_e$ channel with data taking between 1993 and 1998. It made use of neutrinos from a stopped pion source, with energies of $20 < E_\nu < 52.8\,\mathrm{MeV}$ and a short baseline, with the center of the detector 30 m from the neutrino source, corresponding to $L/E_\nu \sim 1\mathrm{m/MeV}$. An excess of events consistent with neutrino oscillation was observed with $\Delta m^2 > 0.2\,\mathrm{eV}^2$ (most favoured region in $0.2 - 2.0\,\mathrm{eV}^2$, although a region around $7\,\mathrm{eV}^2$ also possible)[14]. This excess was significant at more than 3σ.[32]

With a design very similar to LSND, KARMEN did not observe such a signal [31], ruling out the LSND oscillation region with $\Delta m^2 < 10\,\mathrm{eV}^2$, but leaving regions for $\Delta m^2 < 2\,\mathrm{eV}^2$ and around $7\,\mathrm{eV}^2$ compatible with the LSND.[14]

A joint analysis of LSND and KARMEN revealed compatible neutrino oscillation region for Δm^2 in a bend from 0.2 to $1\,\mathrm{eV}^2$ and in a region around $7\,\mathrm{eV}^2$.[14]

MiniBooNE

MiniBooNE, or the Mini Booster Neutrino Experiment, was build to test the results of LSND experiment[14]. It used both neutrinos and antineutrinos with energies of about 500 MeV and about 500 m baseline, yielding the desired $L/E_\nu \sim 1\,\mathrm{m/MeV}$.[32]

Its first result in 2007 reported analysis from a purely neutrino mode, which showed an excellent agreement between data and prediction and excluded the LSND finding at 98% C. L.[10] On the other hand, the results from antineutrino

data, published in 2010, agreed with the LSND findings[32]. Moreover, a combined analysis from 2013 showed an excess at low energies ($< 0.5\,\text{GeV}$) at 3.8σ significance, but the neutrino and antineutrino data were not in perfect accordance. Only if neutrinos were allowed to behave differently than antineutrinos, the results would agree, requiring a CP violating phase and hence more than one sterile neutrino.[32]

The most recent MiniBooNE report from May 31, 2018, summarizes the experiment's findings and reports a total event excess of 4.8σ significance. This excess is shown on fig.4.1. It concludes, that the MiniBooNE data are consistent in energy and magnitude with the excess of events reported by the LSND, and the significance of the combined LSND and MiniBooNE excess is 6.1σ. All of the major backgrounds are constrained by in-situ event measurements, so non-oscillation explanations would need to invoke new anomalous background processes.[30]

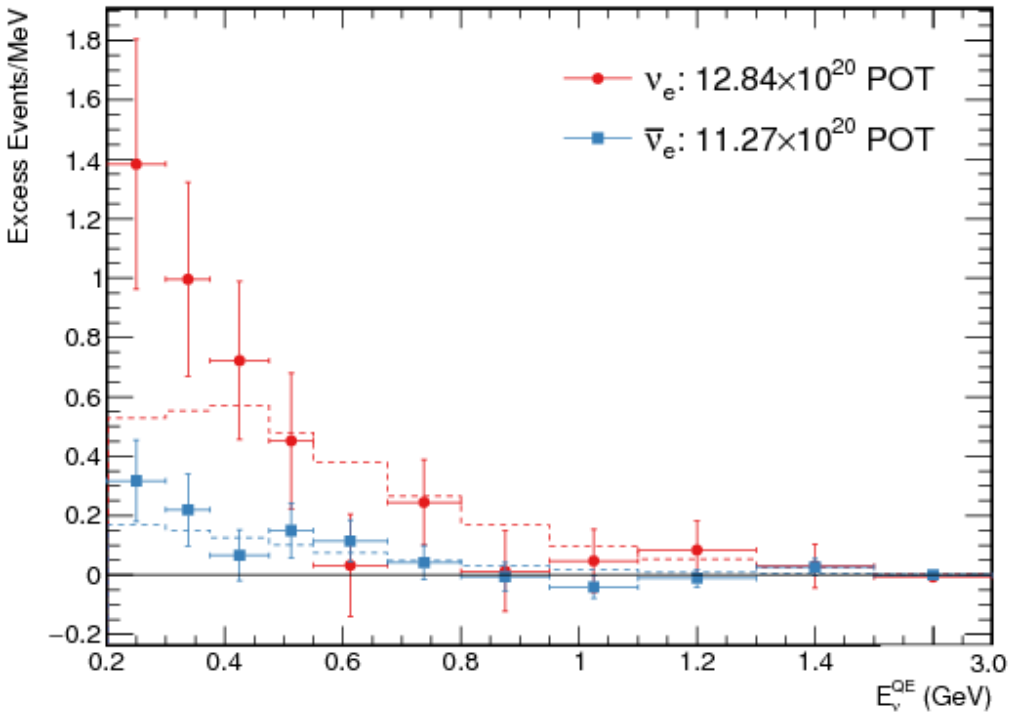

Figure 4.1: The MiniBooNE total ν_e CC quasi-elastic (QE) event excess in both neutrino and antineutrino modes as a function of neutrino energy. Error bars include both statistical and systematic uncertainties. The dashed curves show the best fits to data assuming standard two-neutrino oscillation. Figure is from [30].

4.1.3 Muon (anti)neutrino disappearance experiments

Analysis by atmospheric experiments such as IceCube, DeepCore and SuperKamiokande as well as by experiments searching for charged current (CC) or neutral current (NC) changes, such as MINOS, MINOS+ and NOvA, complement and significantly extend the exclusion regions from the short baseline experiments.[29]

IceCube

The IceCube neutrino observatory is a cubic kilometer Cherenkov neutrino detector in Antarctica, designed to detect high-energy atmospheric and astrophysical neutrinos. It makes use of high-energy atmospheric neutrinos passing through Earth's mantle and core, where they are strongly affected by the MSW effect, which would cause resonant active-sterile oscillations, amplifying a sterile neutrino signature. These neutrinos travel distances of $L < 1.2 \times 10^4\,\mathrm{km}$, with energy in $320\,\mathrm{GeV} < E < 20\,\mathrm{TeV}$, therefore with $L/E \in [0.01, 10]$ m/MeV and hence sensitive to sterile neutrinos of eV masses. DeepCore is an IceCube detector extension, allowing detection of atmospheric neutrinos with energies below 100 GeV.[32]

Experiment established in the mass region around $0.3\,\mathrm{eV}^2$ a limit on $\sin^2(2\theta_{24}) \leq 0.05$ at 99% C.L. and $|U_{\mu 4}|^2 < 0.11$ and $|U_{\tau 4}|^2 < 0.15$ both at 90% C.L.[32]

MINOS and MINOS+

MINOS and MINOS+ are experiments at Fermilab, using the NuMI beam, which was tuned to several different neutrino energies during the runs, allowing a search for sterile neutrino oscillations over a fairly wide range of energies. MINOS is similar to NOvA (described in more detail below) in a sense that they analyse both CC ν_μ and NC disappearance, and they have two detectors, which makes them sensitive to a wide range of Δm^2_{41} values. For MINOS it is $\Delta m^2_{41} \sim 10^{-3} - 10^{-1}\,\mathrm{eV}^2$, wider than for NOvA, because of NOvA's off-axis positioning of the detectors.[29]

MINOS/MINOS+ observed no evidence of mixing between active and sterile neutrinos and provides a stringent limit on θ_{24} for values of Δm^2_{41} above $10^{-2}\,\mathrm{eV}^2$. For $\Delta m^2_{41} = 0.5\,\mathrm{eV}^2$ it sets $\sin^2\theta_{24} < 0.0050$ and $\sin^2\theta_{34} < 0.16$, both at 90% C.L.[33]

4.2 NOvA

There are currently two ways NOvA searches for sterile neutrinos. One is searching for ν_τ appearance in ND, the other is looking for a deficit of neutral-current (NC) neutrino interactions at the FD with respect to the ND prediction. We will (and most of NOvAs sterile neutrino group) focus on the NC channel. It is based on an assumption that ν_s would not interact in the detector, therefore the oscillations into ν_s would result in an energy-dependent suppression of the NC event rate, in contrast to standard oscillations among the three active neutrinos, which leave the NC rate and spectrum unchanged.[21]

NC interactions are mediated by neutral Z_0 boson, which is exchanged primarily with a carbon nucleus. The neutrino leaves the detector with reduced energy and products of nuclear fragmentation remain behind, which appears in the detector as an isolated cluster of energy deposits, distinguishable from the charged-current (CC) interactions by the lack of a charged track, or compact energy deposit, associated with the lepton. Different neutrino interactions in detector are shown on fig.4.2. [21]

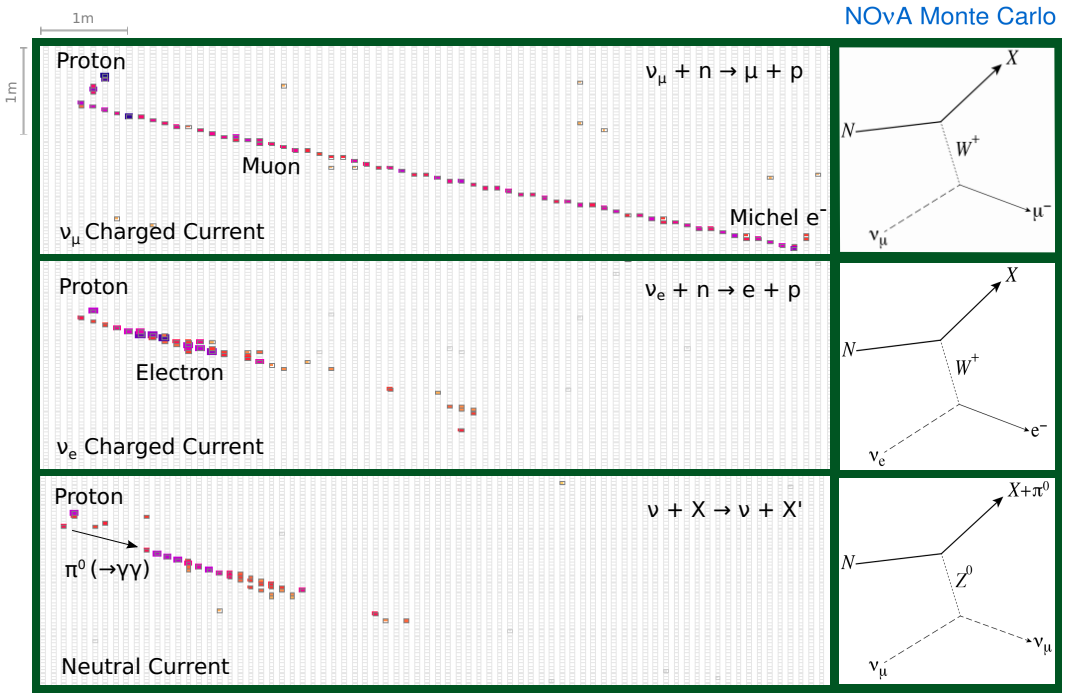

Figure 4.2: Different event topologies in NOvA's detectors with corresponding feynman diagrams. Figure is from [34].

NOvA has a narrow-band beam centred at the three-flavor oscillation maximum, which results in a large expected NC signal with significantly reduced backgrounds providing excellent sensitivity to the θ_{34} mixing angle.[21]

Differences between the ND data and simulation are accounted for by the FD prediction technique. In it, the observed ND spectrum is decomposed into NC, ν_μ CC, and ν_e CC components. To obtain the predicted NC-selected FD spectrum, FD^{pred}, we use far/near ratio extrapolation procedure:

$$FD^{\text{pred}} = \frac{FD^{\text{MC}}}{ND^{\text{MC}}} ND^{\text{data}}, \tag{4.1}$$

where $FD^{\text{MC}}/ND^{\text{MC}}$ is the ratio of FD and ND Monte Carlo simulation and ND^{data} is the ND data. Oscillation probability weights are applied to each FD predicted components. This extrapolation prediction is compared with the FD data (FD^{data}) and any further data Monte Carlo simulation difference is absorbed as systematic uncertainties.[35]

To test for active to sterile neutrino mixing we use a model independent variable R_{NC}:

$$R_{\text{NC}} \equiv \frac{FD^{\text{data}} - \sum FD^{\text{pred}}\,(\text{bkg})}{FD^{\text{pred}}\,(\text{NC})}, \tag{4.2}$$

where $\sum FD^{\text{pred}}\,(\text{bkg})$ is the sum of the predictions of backgrounds at the FD. All the predicted quantities are calculated assuming three-flavor oscillations. Active to sterile neutrino mixing would result in $R_{\text{NC}} < 1$.[35]

4.2.1 First NOvA sterile neutrino analysis

First analysis of a light ν_s search using a NC channel uses data collected from February 2014 to May 2016, corresponding to beam powers ranging between 250 and 560 kW. It is also the only analysis whose results were published (see ref. [21]) in time of completing this thesis. During this time, the experiment collected 6.68×10^{20} protons-on-target (POT), equivalent to a full-detector exposure of 6.05×10^{20} POT.[21]

It is a rate-only measurement which compares the FD NC rate to unoscillated and oscillated predicted rates. This is valid for $0.05 \leq \Delta m^2_{41} \leq 0.5\,\mathrm{eV}^2$, where the analysis is not sensitive to oscillations affecting the rates in the ND, present at larger Δm^2_{41} values. Within this range, the analysis is also insensitive to degenerate solutions with the three-flavor model, occurring when $\Delta m^2_{41} \simeq \Delta m^2_{32}$.[21]

There were 95 NC event candidates at the FD observed, compared with $83.5 \pm 9.7\,(\mathrm{stat}) \pm 9.4\,(\mathrm{syst})$ events predicted under the three-flavor oscillation assumption. The value of R_{NC} was measured to be $R_{NC} = 1.19 \pm 0.16\,(\mathrm{stat}) + 0.10\,(\mathrm{syst})$, corresponding to a 1.03σ excess over the three-flavor prediction of $R_{NC} = 1$, and consistent with three-flavor neutrino oscillations.[21]

This event count was predicted to contain 60.6 ± 7.4 NC signals, 4.6 ± 0.7 ν_μ, 3.6 ± 0.6 ν_e and 0.4 ± 0.1 ν_τ background and 14.3 ± 0.7 cosmic background.[21]

Values of 3 neutrino flavor mixing parameters were taken from the 2014th edition of Particle data groups "The review of particle physics", with normal hierarchy and maximal mixing assumed, including matter effects and setting δ_{CP} to 0 since its effect is negligible.[21]

To be able to compare to other experiments or other channels, the $3 + 1$ neutrino flavor model was used, with same conventions that were used above in chapter 2, including accounting for matter effects. The NC sample is sensitive to θ_{24} , θ_{34} , and δ_{24}. Result of this analysis are limits of $\theta_{24} < 20.8°$ and $\theta_{34} < 31.2°$, obtained at the 90% C.L. (confidence level). Expressed in terms of the relevant matrix elements, these limits become $|U_{\mu 4}|^2 < 0.126$ and $|U_{\tau 4}|^2 < 0.268$ at the 90% C.L., where a $\cos^2\theta_{14} = 1$ was assumed in both cases. These constrains are visualised in fig.4.3 and fig.4.4, where we can see that obtained limits are not yet competitive with the world's best limits.[21]

Systematic uncertainties

Systematic uncertainties for NC event rate in the FD were evaluated one parameter at a time. Sets of modified simulated events were propagated through the full extrapolation and analysis chain, producing shifted FD predictions. Deviations from the nominal prediction at the FD was than used as the uncertainty. Uncertainties affecting both detectors in the same way (absolute uncertainties) largely cancel in this analysis. There are also uncertainties specific to either one of the detectors (relative uncertainties) which do not cancel and contribute to the overall systematic error.[21]

The largest systematic uncertainty comes from mismodelling of the signal in the ND. To asses the size of this uncertainty, the observed data-MC discrepancy was assigned to either NC or ν_μ events and propagated to the FD, while assuming a 100% scale uncertainty on the small ν_e CC component. As a result a 7.0% uncertainty was assigned on the NC signal and a 10.4% uncertainty on

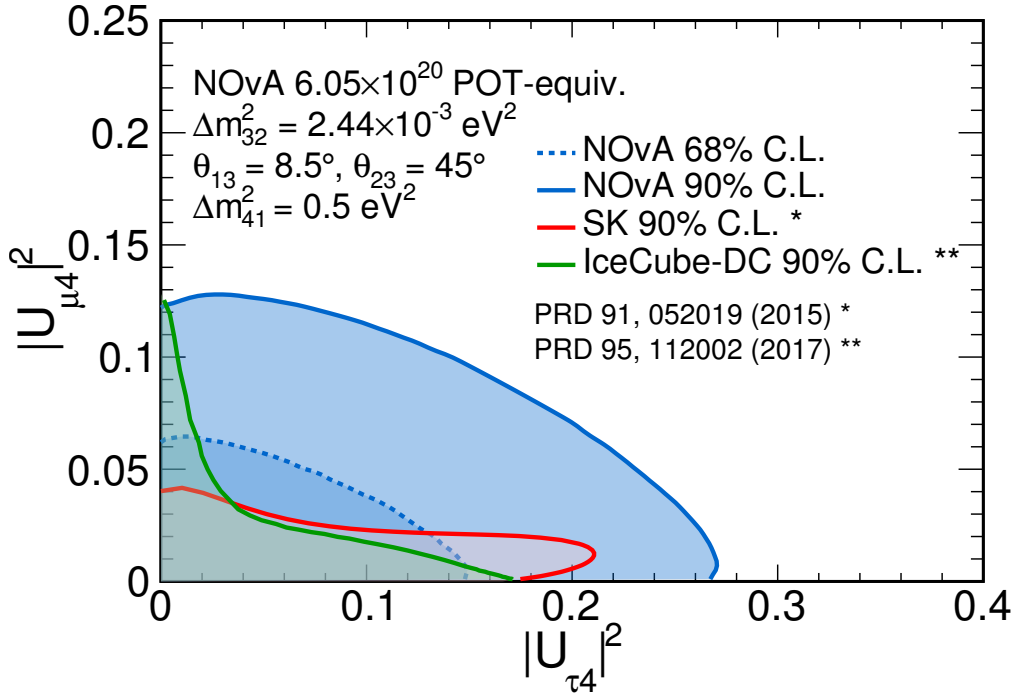

Figure 4.3: Two dimensional graph of non-excluded regions (shaded in blue) at 68% and 90% C.L. in terms of $|U_{\mu 4}|^2$ and $|U_{\tau 4}|^2$ where we assume $\cos^2\theta_{14} = 1$ in both cases, for depicted exposure, POT-equivalent, and oscillation parameters. Comparison to SuperK (2015) and IceCube (2017) 90% C.L. excluded (resp. non-excluded) regions. Figure is from [21].

the CC backgrounds[21]. This is a very conservative method, since the data-MC discrepancy is fully covered by other uncertainties.[36]

The second largest source of uncertainties is a 5% uncertainty on the calibrations between the detectors, which was conservatively applied as both an absolute and relative uncertainty. It leads to a 5.8% uncertainty on the NC signal and a 6.0% uncertainty on the CC backgrounds in the FD. It was determined through observing data-simulation differences in several probes including Michel electrons and the measured π^0 mass peak.[21]

A normalization systematic arises from reconstruction inefficiencies due to multiple interactions in the detector per beam pulse resulting in 4.9% uncertainty for both NC signal and CC background. The deep inelastic scattering effect results in a 1.6% NC signal uncertainty and a 4.8% CC background uncertainty.[21]

Other sources of systematic uncertainties include uncertainties on the cross section, the three-flavor parameters, the detector noise model, the mass of the detector, the POT counting, the variation of the beam intensity, the beam flux model, the effect of using limited statistics for the simulation, the modelling of scintillator response, the normalization of the modelling of CC scattering from correlated nucleons, the possible contamination of the ND spectrum by events originating in materials outside of the detector, and potential mismodeling of acceptance differences between the ND and FD due to their differing sizes.[21]

The result of a sum in quadrature of all effect is a 12.2% uncertainty on the NC signal and a 15.3% uncertainty on the CC background.[21]

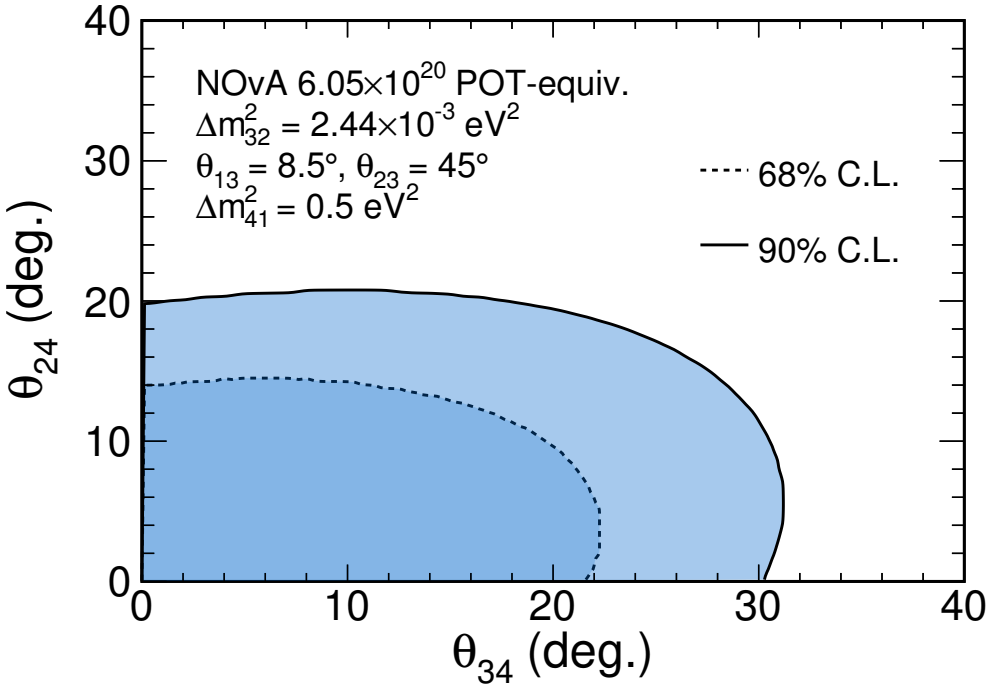

Figure 4.4: Two dimensional graph of non-excluded regions (shaded) at 68% and 90% C.L. in terms of θ_{24} and θ_{34} for depicted exposure, POT-equivalent, and oscillation parameters. Figure is from [21].

NC selection

The CVN was used as a primary selector for NC events, along with a set of selection cuts and a boosted decision tree employed for cosmic background rejection [35]. Since the FD is at the ground level, cosmic rays are a major background. On average, before applying selections, 74000 cosmogenic events were reconstructed for each reconstructed neutrino event in the 10 µs beam spill window at the FD. Other source of background are misidentified CC neutrino interactions. Since the ND is located underground, cosmogenic background is negligible, but NuMI beam events interacting in the periphery of the ND and in the surrounding cavern provide another source of background.[21]

NC selection used mostly shower-based cuts for NC identification, but for cosmic rejection, tools developed for the ν_μ group were used, which had an undesirable consequence that all NC-selected events were required to have at least one Kalman-reconstructed track.[36]

The NC selection can be divided into several stages:[36]

1. Slice-based cuts: These include beam and data quality cuts, timing cuts and diblock mask cuts.[36]

2. Event quality cuts: All events were required to have a reconstructed vertex and at least one reconstructed prong that spans a minimum of two detector planes.[21]

3. Containment cuts: The entirety of the prong is required to be at least 10 cm (25 cm) away from the FD (ND) walls.

4. NC/CC separation cuts: CVN was used to separate NC, CC and cosmogenic interactions, using a value of 0.2 and the minimum number of 20 hits required .[21]

5. Cosmic rejection cuts: No algorithm was specifically trained to remove these, instead, to remove cosmogenic neutron backgrounds in the FD, the reconstructed start and end position of prongs had to be a minimum distance of 5 m away from the top of the detector; to remove downward-going cosmogenic activity, the fractional transverse momentum, with respect to the beam direction, of the highest energy prong was required to be less than 0.8; and, finally, to remove the remaining contained cosmogenic backgrounds, a boosted decision tree was employed. The application of cosmic rejection cuts is illustrated on fig.4.5. A rejection level where only 1 in every 1.7 million cosmogenic events was misidentified as a NC signal event was obtained.[21]

6. Energy cut: All events were required to have a calorimetric energy between 0.5 and 4 GeV. This criterion rejects low-energy events, where combined uncertainties in energy resolution and threshold are substantial, and avoids higher-energy regions where the ND and FD selection efficiencies diverge due to the smaller size of the ND.[21]

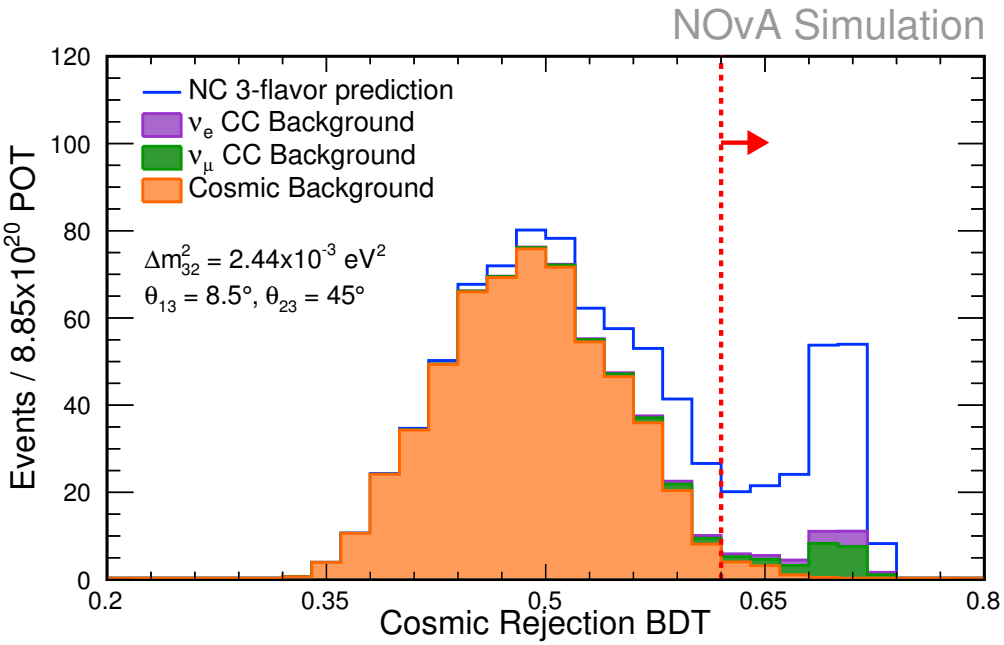

Figure 4.5: A Monte Carlo comparison plot for the NC cosmic rejection boosted decision tree (BDT) distribution. It is a stacked plot showing the event distribution at the NOvA's FD, that passes through the NC selection, but not including the cut on the NC cosmic rejection BDT variable, which is displayed as a red red line. MC is normalised to the data of 8.85×10^{20} POT-equivalent using the displayed parameters values. Figure is from NOvA's internal database.

After all selections, the effective fiducial mass of the FD (ND) is 8.83 kt (34 t)[21] and a 50% (62%) NC efficiency and 72% (70%) NC signal purity was achieved in the fiducial volume.[35]

4.2.2 2017 sterile neutrino analysis

The 2017 analysis uses data taken from the beginning until January, 10 2017, with full-detector-equivalent exposure expected to be close to 9×10^{20} POT for FD and 8.05×10^{20} POT for ND. This corresponds to a 50% increase in statistics over the 2016 analysis.[36]

The main changes from the 2016 analysis include fitting of the NC reconstructed energy instead of a rate-only counting, improved cosmic rejection, improved NC visible energy resolution, 50% improvement to the NC selection efficiency, MC improvements (namely an upgrade of Genie and Geant, improvement in noise modelling, in inclusion of Cherenkov light, in flux), improvements in MC cross section modelling and adding new systematic uncertainties for the improved selection and simulation.[36]

In the first analysis, the energy was corrected with a scale factor extracted from studies of leptonic interactions, which was shown to overestimate the NC visible energy by nearly a factor of two. Therefore a new correction factor was determined, separate for both the ND and the FD. This new corrected energy is newly referred to as Visible energy.[36]

The NC selection has been updated to be based mostly on prongs, increasing efficiency and removing dependencies on selections and pre-selections defined from ν_μ and ν_e groups. Shower and track requirements were removed and the maximum distance of all prongs to the nearest edge was modified to 35 cm (50 cm) for the ND (FD), except for the top of the FD, where the minimum distance required is 100 cm. The CVN NC selections minimum number of hits was increased from 20 to 25. The new range for the Visible energy criterion was set from 250 MeV to 10 GeV. To allow comparison, the 2016 Calorimetric energy criterion can be converted to a Visible energy range of 0.3 to 2.5 GeV. [36]

The selection in the 2017 analysis achieves a 50% increase in the selected signal and 60% reduction in cosmics from the 2016 analysis. The efficiency and purities for the FD (ND) are 52% (50%) and 77% (67%), respectively. This can not be however compared to the numbers quoted for the 2016 analysis, which included a fiducial cut and required a track and LID shower. Removing these track and LID shower pre-selection cuts has greatly improved our overall efficiency.[36]

Conclusion

In the beginning we presented a summary of neutrino history to provide context for the study of neutrino oscillations and sterile neutrinos and to introduce reader to the aspects of neutrinos.

We showed a description of neutrino oscillations, first applying the 3 active-neutrino model in a vacuum, than considering matter effects on the propagation of neutrino and therefore on oscillation probabilities. We listed up-to-date values of the properties of neutrinos and neutrino oscillations. Than we discussed adding sterile neutrino(s) and focusing on the 3 active + 1 sterile neutrino model we expressed several often used probabilities.

We showed, that sterile neutrinos are (and were) studied on many experiments all around the world and in all types of neutrino study, be it a study of atmospheric, solar, reactor, accelerator, or other neutrinos. This topic is now very much alive and many new and often ground-breaking results come out every year. We listed and described the most interesting of these experiments, including the NOvA experiment on which we focused in more detail.

We described NOvA's components and used methods, as well as its first (and partially second) analysis of the neutral current disappearance in the far detector, which is a method it uses to search for sterile neutrinos. We had to conclude that NOvA in its first neutral current analysis did not find any evidence of sterile neutrinos and was able to provide constraints on the oscillation parameters in case of the 3+1 neutrino model. These constraints are however not yet competitive with the limits from other experiments, but will with high certainty improve with better statistics, which would add NOvA to the group of the most influencing experiments in the topic of sterile neutrinos.

Bibliography

[1] L. M. Brown. The idea of the neutrino. *Physics Today*, 31(9):23–28, September 1978. doi: 10.1063/1.2995181.

[2] E. Amaldi. From the discovery of the neutron to the discovery of nuclear fission. *Physics Reports*, 111(1-4):1–331, 1984. doi: 10.1016/0370-1573(84)90214-X.

[3] F. T. Avignone & S. R. Elliott & J. Engel. Double beta decay, majorana neutrino, and neutrino mass. *Reviews of modern physics*, 80(2):481–516, April-June 2008. doi: 10.1103/RevModPhys.80.481. arXiv:0708.1033.

[4] K. Zuber. *Neutrino Physics*. Series in High Energy Physics, Cosmology and Gravitation. CRC Press, second edition, August 2011. ISBN 978-1-4200-6471-1.

[5] The official web site of the nobel prize. URL `https://www.nobelprize.org/`. Cited 04.2018.

[6] M. C. Goodman. Resource letter anp-1: Advances in neutrino physics. *American Journal of Physics*, 84:309–319, 2016. doi: 10.1119/1.4962228.

[7] Particle Data Group (C. Patrignani et al.). Review of particle physics. *Chin. Phys.*, C40(10):100001, 2016. doi: 10.1088/1674-1137/40/10/100001. 14. Neutrino Masses, Mixing, and Oscillations: updated November 2017.

[8] DONUT Collaboration. Observation of tau neutrino interactions. 2000. doi: 10.1016/S0370-2693(01)00307-0. arXiv:hep-ex/0012035.

[9] G. K. Kafka. *A search for sterile neutrino at the NOvA far detector*. PhD thesis, Harvard University, May 2016.

[10] A. A. Aguilar-Arevalo et al. Search for electron neutrino appearance at the $\delta m^2 \sim 1\text{eV}^2$ scale. *Physical Review Letters*, 98, June 2007. doi: 10.1103/PhysRevLett.98.231801.

[11] A. Strumia. Interpreting the lsnd anomaly: sterile neutrinos or cpt-violation or...? *Physics Letters B*, 539(1-2):91–101, July 2002. doi: 10.1016/S0370-2693(02)02042-7.

[12] S. Mondal. Physics of neutrino oscillations. Nov 2015. arXiv:1511.06752.

[13] P. Lipari. Introduction to neutrino physics. In *2001 CERN-CLAF School of high-energy physics, Itacuruca, Brazil, 6-19 May, 2001: Proceedings*, pages 115–199, 2001. URL `http://cdsweb.cern.ch/search.py?sysno=002238801CER`.

[14] J. A. Thomas & P. L. Vahle. *Neutrino oscillations, present status and future plans*. World Scientific, 2008. ISBN 13 978-981-277-196-4.

[15] Susanne Mertens. *Background Processes in the Electrostatic Spectrometers of the KATRIN Experiment*. Springer Science & Business Media, 01 2014. ISBN 3319011774. doi: 10.1007/978-3-319-01177-6˙2.

[16] O. Mena & S. Parke. Unified graphical summary of neutrino mixing parameters. *Physical Review D*, 69(11), 2003. doi: 10.1103/PhysRevD.69.117301. arXiv:hep-ph/0312131.

[17] M. Sorel & J. M. Conrad & M. H. Shaevitz. Combined analysis of short-baseline neutrino experiments in the 3+1 and 3+2 sterile neutrino oscillation hypotheses. *Physical Review D*, 70(073004), April 2004. doi: 10.1103/PhysRevD.70.073004.

[18] S Gariazzo & C. Giunti & M. Laveder & Y. F. Li. Updated global 3+1 analysis of short-baseline neutrino oscillations. 2017. doi: 10.1007/JHEP06(2017)135. arXiv:1703.00860.

[19] M Maltoni, T Schwetz, and J.W.F Valle. Cornering (3+1) sterile neutrino schemes. *Physics Letters B*, 518(3):252 – 260, 2001. ISSN 0370-2693. doi: https://doi.org/10.1016/S0370-2693(01)01068-1. URL http://www.sciencedirect.com/science/article/pii/S0370269301010681.

[20] J. Kopp & P. A. N. Machado & M. Maltoni & T. Schwetz. Sterile neutrino oscillations: The global picture. 2013. doi: 10.1007/JHEP05(2013)050. arXiv:1303.3011.

[21] P. Adamson et al. Search for active-sterile neutrino mixing using neutral-current interactions in nova. *Phys. Rev.*, D96(7), 2017. doi: 10.1103/PhysRevD.96.072006. arXiv:1706.04592.

[22] D. S. Ayres et al. The nova technical design report. *NOvA Collaboration*, 2007. doi: 10.2172/935497.

[23] Nova fermilab official homepage. URL https://www-nova.fnal.gov/how-nova-works.html. Cited 04.2018.

[24] P. Adamson et al. The numi neutrino beam. 2015. doi: 10.1016/j.nima.2015.08.063. arXiv:1507.06690.

[25] L. Ren et al. Measurement of the antineutrino to neutrino charged-current interaction cross section ratio in minerva. *Phys. Rev.*, D95(7), 2017. doi: 10.1103/PhysRevD.97.019902. arXiv:1701.04857.

[26] T. Xinchun for the collaboration. Nova data acquisition software system. arXiv:1109.6825.

[27] Yury Kudenko. Proceedings, international conference on instrumentation for colliding beam physics (instr17): Novosibirsk, russia. *JINST*, 12(06), 2017. doi: 10.1088/1748-0221/12/06/C06003. arXiv:1705.06059.

[28] A. Aurisano et al. A convolutional neural network neutrino event classifier. *JINST*, 11(09), 2016. doi: 10.1088/1748-0221/11/09/P09001. arXiv:1604.01444.

[29] M. Dentler et al. Updated global analysis of neutrino oscillations in the presence of ev-scale sterile neutrinos. (MITP/18-023, FERMILAB-PUB-18-086-T, IFT-UAM/CSIC-18-033), 2018. arXiv:1803.10661.

[30] A. A. Aguilar-Arevalo et al. Observation of a significant excess of electron-like events in the miniboone short-baseline neutrino experiment. 2018. arXiv:1805.12028.

[31] Antonio Palazzo. Short- and long-baseline sterile neutrino phenomenology. In *Proceedings, Prospects in Neutrino Physics (NuPhys2016): London, UK, December 12-14, 2016*, 2017. URL http://inspirehep.net/record/1598131/files/arXiv:1705.01592.pdf. arXiv::1705.01592.

[32] Julia Haser. Light sterile neutrino searches. In *29th Rencontres de Blois on Particle Physics and Cosmology Blois, France, May 28-June 2, 2017*, 2017. URL https://inspirehep.net/record/1631177/files/arXiv:1710.06330.pdf. arXiv:1710.06330.

[33] P. Adamson et al. Search for sterile neutrinos in minos and minos+ using a two-detector fit. *Phys. Rev. Lett.*, 2017. arXiv:1710.06488.

[34] Kanika Sachdev. A data-driven method of background prediction at nova. In *Meeting of the APS Division of Particles and Fields (DPF 2013) Santa Cruz, California, USA, August 13-17, 2013*, 2013. URL http://inspirehep.net/record/1256324/files/arXiv:1310.0119.pdf. arXiv:1310.0119.

[35] S. Edayath et al. Sterile neutrino search in the nova far detector. In *Meeting of the APS Division of Particles and Fields (DPF 2017) Batavia, Illinois, USA, July 31-August 4, 2017*, 2017. URL http://lss.fnal.gov/archive/2017/conf/fermilab-conf-17-516-nd.pdf. arXiv:1710.01280.

[36] A. Sousa and L. Suter on behalf of the NC/Sterile Working Group. Neutral current executive summary 2017. internal NOvA document, DocDB-22514, August 2017.

List of Figures

List of Tables

List of Abbreviations

SNU	Solar Neutrino Unit
PMNS	Pontecorvo-Maki-Nakagawa-Sakata
CPT	Charge-Parity-Time
CC	Charged current
NC	Neutral current
MSW	Mikheyev-Smirnov-Wolfenstein
C.L.	Confidence Level
SBL	Short Baseline
ND	Near Detector
FD	Far Detector
NOvA	NuMI Off-axis ν_e Appearance experiment
NuMI	Neutrino at the Main Injector
MINOS	Main Injector Neutrino Oscillation Search
DUNE	Deep Underground Neutrino Experiment
FHC	Forward Horn Current
RHC	Reversed Horn Current
POT	Protons On Target
WLS	Wavelength Shifting fibres
APD	Avalanche Photodiode
DAQ	Data Acquisition
PID	Particle Identification
CVN	Convolutional Visual Network
LSND	Liquid Scintillation Neutrino Detector
MiniBooNE	Mini Booster Neutrino Experiment
DANSS	Detector of Anti-Neutrino based on Solid Scintillator
NEOS	Neutrino Oscillation at Short baseline
GALLEX	Gallium Experiment
SAGE	Soviet-American Gallium Experiment
KARMEN	Karlsruhe-Rutherfor intermediate Energy Neutrino experiment
NOMAD	Neutrino Oscillation Magnetic Detector
ICARUS	Imaging Cosmic And Rare Underground Signals
OPERA	Oscillation Project with Emulsion-Tracking Apparatus
K2K	KEK to Kamioka
CNGS	CERN Neutrinos to Gran Sasso
IMB	Irvine-Michigan-Brookhaven
QE	Quasi-elastic
BDT	Boosted Decision Tree
PRG	Physical Review D
MC	Monte Carlo